

Multi-scale evaluation of global gross primary productivity and evapotranspiration products derived from Breathing Earth System Simulator (BESS)



Chongya Jiang^a, Youngryel Ryu^{a,b,c,d,*}

^a Research Institute of Agriculture and Life Sciences, Seoul National University, Republic of Korea

^b Department of Landscape Architecture and Rural Systems Engineering, Seoul National University, Seoul, Republic of Korea

^c Interdisciplinary Program in Agricultural and Forest Meteorology, Seoul National University, Republic of Korea

^d Interdisciplinary Program in Landscape Architecture, Seoul National University, Republic of Korea

ARTICLE INFO

Article history:

Received 22 March 2016

Received in revised form 16 August 2016

Accepted 30 August 2016

Available online 28 September 2016

Keywords:

Gross primary productivity

Evapotranspiration

BESS

Global

MPI-BGC

MODIS

ABSTRACT

Several global gross primary production (GPP) and evapotranspiration (ET) remote sensing products exist, mainly provided by machine-learning (e.g. MPI-BGC) and semi-empirical (e.g. MODIS) approaches. Process-based approaches have the advantage of representing the atmosphere-vegetation-soil system and associated fluxes as an organic integration, but their sophistication results in a lack of high spatiotemporal resolution continuous products. Targeting this gap, we reported a new set of global 8-day composite 1-km resolution GPP and ET products from 2000 to 2015, using a simplified process-based model, the Breathing Earth System Simulator (BESS). BESS couples atmosphere and canopy radiative transfer, photosynthesis and evapotranspiration, and uses MODIS atmosphere and land data and other satellite data sources as inputs. We evaluated BESS products against FLUXNET observations at site scale (total of 113 sites, 742 site years), and against MPI-BGC products at global scale. At site scale, BESS 8-day products agreed with FLUXNET observations with $R^2 = 0.67$ and $RMSE = 2.58 \text{ gC m}^{-2} \text{ d}^{-1}$ for GPP, and $R^2 = 0.62$ and $RMSE = 0.78 \text{ mm d}^{-1}$ for ET, respectively, and they captured a majority of seasonal variability, about half of spatial variability, and a minority of interannual variability in FLUXNET observations. At global scale, BESS mean annual sum GPP and ET maps agreed with MPI-BGC products with $R^2 = 0.93$ and $RMSE = 229 \text{ gC m}^{-2} \text{ y}^{-1}$ for GPP, and $R^2 = 0.90$ and $RMSE = 118 \text{ mm y}^{-1}$ for ET, respectively. Over the period of 2001–2011, BESS quantified the mean global GPP and ET as $122 \pm 25 \text{ PgC y}^{-1}$ and $65 \times 10^3 \pm 11 \times 10^3 \text{ km}^3 \text{ y}^{-1}$, respectively, with a significant ascending GPP trend by 0.27 PgC y^{-2} ($p < 0.05$), similar to MPI-BGC products as well. Overall, BESS GPP and ET estimates were comparable with FLUXNET observations and MPI-BGC products. The process-based BESS can serve as a set of independent GPP and ET products from official MODIS GPP and ET products.

© 2016 Elsevier Inc. All rights reserved.

1. Introduction

Machine-learning and semi-empirical approaches are two ways to derive regional and global gross primary production (GPP) and evapotranspiration (ET) from remote sensing data. Machine-learning approaches upscale site-observed fluxes to a larger scale by establishing statistical models, with satellite-derived parameters and other explanatory variables (Beer et al., 2010; Jung et al., 2010). Semi-empirical approaches utilize equations with a concise physiological meaning that are parameterized with several empirical constraint functions or vegetation indices (Wang et al., 2010; Yebra et al., 2015). For effectiveness and efficiency, two global time-series GPP and ET products – derived

from a machine-learning approach (the Max Planck Institute for Biogeochemistry, MPI-BGC) (Jung et al., 2011) and a semi-empirical approach (the MODerate-resolution Imaging Spectroradiometer, MODIS) (Mu et al., 2011; Zhao et al., 2005) – have become widely used.

Integrating remote sensing data with process-based models provides another way to generate global GPP and ET datasets (Plummer, 2000; Sellers et al., 1995). Process-based models use a series of nonlinear equations to represent the atmosphere-vegetation-soil system and associated fluxes (Dai et al., 2003; Dickinson, 1983). Compared with machine-learning and semi-empirical models, process-based models are able to provide deeper insights into underlying inter-action mechanisms and their synergetic responses to environmental change (Shao et al., 2013a; Yang et al., 2011). Advances in remote sensing that occurred in the 2000s have provided further relevant information regarding the atmosphere and land surface, enabling the biogeoscience community to verify (Ichii et al., 2013; Mao et al., 2012) and drive (Lawrence and

* Corresponding author at: Department of Landscape Architecture and Rural Systems Engineering, Seoul National University, Seoul 151-921, Republic of Korea.
E-mail address: yryu@snu.ac.kr (Y. Ryu).

Chase, 2007; Senay et al., 2013) process-based models, to optimize them through assimilation (Fang et al., 2011; Hazarika et al., 2005), as well as to refine and improve semi-empirical models (Sasai et al., 2005; Zhang et al., 2012). However, process-based models are usually associated with sophistication (Rodell et al., 2015). This feature results in a lack of publically-available global and continuous high spatiotemporal resolution GPP and ET products, derived from a process-based satellite-driven approach.

The Breathing Earth System Simulator (BESS), is a concise process-based model designed to continuously monitor and map carbon and water fluxes with fine spatial (1–5 km) and temporal (8-daily composite) resolution at global scale (Ryu et al., 2011). It is highly simplified, only coupling a 1-dimensional atmosphere radiative transfer module, a two-leaf canopy radiative transfer module, and an integrated carbon assimilation – stomatal conductance – energy balance module. Uniquely, it is designed to be most sensitive to the variables that can be quantified reliably, taking full advantages of MODIS atmospheric and land products. By using MODIS aerosol, cloud and atmospheric profile information, BESS computes 5 km resolution radiation, temperature and humidity data to drive land surface modules. In contrast, MODIS GPP and ET products use $1.00^\circ \times 1.25^\circ$ resolution meteorological forcing data from the Data Assimilation Office (DAO) (Mu et al., 2011; Zhao et al., 2005), and MPI-BGC GPP and ET products use 0.5 resolution temperature and precipitation data from Climate Research Unit (CRU), notwithstanding that the coarse resolution could cause large uncertainties (Sasai et al., 2005; Yuan et al., 2010). In addition, BESS quantifies the flux contributions from sunlit/shaded canopy through the explicit computation of direct/diffuse radiation in the atmosphere and canopy radiative transfer. This has been proven to be of great importance (Chen et al., 2016, 2012; Donohue et al., 2014), but is not the case for most global GPP and ET satellite-derived datasets (Jung et al., 2011; Yebra et al., 2013, 2015; Yuan et al., 2010).

Past evaluations of BESS were limited in their spatial or temporal scales. At site level, Ryu et al. (2011) showed that BESS GPP and ET agreed with site-observed fluxes (33 sites, 33 site years) over various land cover types and climate zones. Whitley et al. (2016) compared the GPP and ET estimates derived from six process-based models with five Australian savanna flux towers datasets, and showed that BESS well captured the seasonal trajectory of GPP and ET in that complex terrestrial biome. Keenan et al. (2012) investigated the capability of 16 terrestrial biosphere models and three remote sensing models for capturing the interannual variability of GPP at 11 forested sites in North America, demonstrating that BESS performed well in deciduous broadleaf forests but poor in evergreen broadleaf forests. At regional and global level, Song et al. (2014) showed that BESS ET is in line with the water balance estimation, both monthly and annually, at a Korean basin. Ryu et al. (2011) showed that BESS mean annual GPP and ET between 2001 and 2003 agreed well with machine-learning products (Beer et al., 2010; Jung et al., 2010) over 24 climate zones. However, these assessments were still in the initial stages. At site level, BESS accuracy was only quantified from a small set of sites, and a comparison with other spatially and temporally consistent products was not conducted. At global level, BESS performance was not systematically characterized through an intensive map-to-map intercomparison, and more importantly, over a long time span. According to the definition given by the Committee on Earth Observation Satellites (CEOS) Land Product Validation (LPV) subgroup (<http://lpvs.gsfc.nasa.gov/>), these efforts can only be considered as Stage 1 validation in a four-stage hierarchy. Therefore, a more comprehensive Stage 2 evaluation, involving a significant set of locations and time periods and spatial and temporal consistency with similar products, is required.

The objectives of this study were threefold: (1) to present global GPP and ET products in 1-km spatial resolution and 8-day composite from 2000 to 2015, (2) to evaluate the performance of BESS products by direct comparison with 113 site observations in a newly-released FLUXNET 2015 dataset, and (3) to characterize the spatiotemporal

patterns of BESS products by an intercomparison with two independent products, MPI-BGC and MODIS. We provide a distinct global and continuous high spatiotemporal resolution GPP and ET products, derived from a process-based satellite-driven approach, instead of widely-applied machine-learning and semi-empirical approaches. Moreover, we move forward to the Stage 2 validation by conducting comprehensive analysis at two spatial scales (site and global) and four temporal scales (8-day, monthly, annual, and decadal).

2. Materials and methods

2.1. BESS GPP and ET products

We produced BESS 8-day composite 1-km resolution GPP and ET products using multi-satellite remote sensing data from 2000 to 2015. Fig. 1 showed the flowchart of the core algorithm. An atmospheric radiative transfer model, Forest Light Environmental Simulator (FLIES) (Kobayashi and Iwabuchi, 2008; Ryu et al., 2011), computed direct and diffuse radiation in the photosynthetically active radiation (PAR) and near infrared (NIR) spectral domains. A two-leaf and two-stream canopy radiative transfer model (De Pury and Farquhar, 1997; Ryu et al., 2011) computed the absorbed PAR and NIR radiation by sunlit and shade canopy. A plant functional type (PFT) dependent look-up table (LUT) quantified maximum leaf carboxylation capacity at 25 °C (V_{max}^{25C}), according to the TRY leaf trait database (Kattge et al., 2009, 2011) (Table A1), and the leaf-level V_{max}^{25C} were further upscaled to sunlit/shade canopy V_{max}^{25C} (Ryu et al., 2011). Ambient and saturated vapor pressure, air specific heat and clear-sky emissivity were calculated from temperature, humidity and pressure data. Subsequently, a carbon-water-coupled module which incorporated a two-leaf longwave radiative transfer model (Wang et al., 2006), Farquhar's photosynthesis model for C3 and C4 plants (Collatz et al., 1992; Farquhar et al., 1980), a stomatal conductance equation (Ball, 1988), and the quadratic Penman-Monteith and energy balance equations (Paw U and Gao, 1988; Paw U, 1987), computed GPP and ET for sunlit and shade canopy as well as soil evaporation through an iterative procedure. Five intermediate variables, sunlit leaf temperature, shade leaf temperature, soil temperature, intercellular CO₂ concentration, and aerodynamic resistance, were solved in the iteration. The derived instantaneous estimates of GPP and ET were finally temporally upscaled to 8-day mean estimates using a simple cosine function (Ryu et al., 2012a). Compared with the previous version (Ryu et al., 2011), the improved algorithm treated intercellular CO₂ concentration dynamically and better accounted for sunlit/shade canopy longwave radiation balance (Appendix A).

In total, BESS products used seven MODIS atmosphere (Collection 6) and land (Collection 5) products, four other satellite datasets, four re-analysis datasets, and three ancillary datasets as input data. The global 1-km resolution land mask was first determined by synthesizing the MCD12Q1 yearly land cover type product between 2001 and 2013 (Friedl et al., 2010), yielding a total land area of 133,666,330 km², excluding Antarctica and inland water. The geographic coordinates for each land grid pixel were calculated according to the MODIS sinusoidal reprojection model used by all MODIS land products (Wolfe et al., 1998). We subsequently used the nearest neighborhood resampling approach to reproject swaths of MOD04_L2 aerosol (Remer et al., 2005), MOD06_L2 cloud (Platnick et al., 2003) and MOD07_L2 atmosphere profile (Seemann et al., 2003) products to 5-km resolution sinusoidal global land grids. The computed radiation components using these MODIS atmosphere products were further resampled to 1 km resolution by the nearest neighborhood resampling approach. MOD11A1 land surface temperature (LST) product (Wan, 2008), gap-filled with surface temperature embedded in MOD06_L2 product, was used as an initial guess of sunlit/shade temperature and soil temperature. MCD15A2 leaf area index (LAI) product (Shabanov et al., 2005), the most sensitive data for fluxes estimation (Ryu et al., 2011), was filtered using a simple

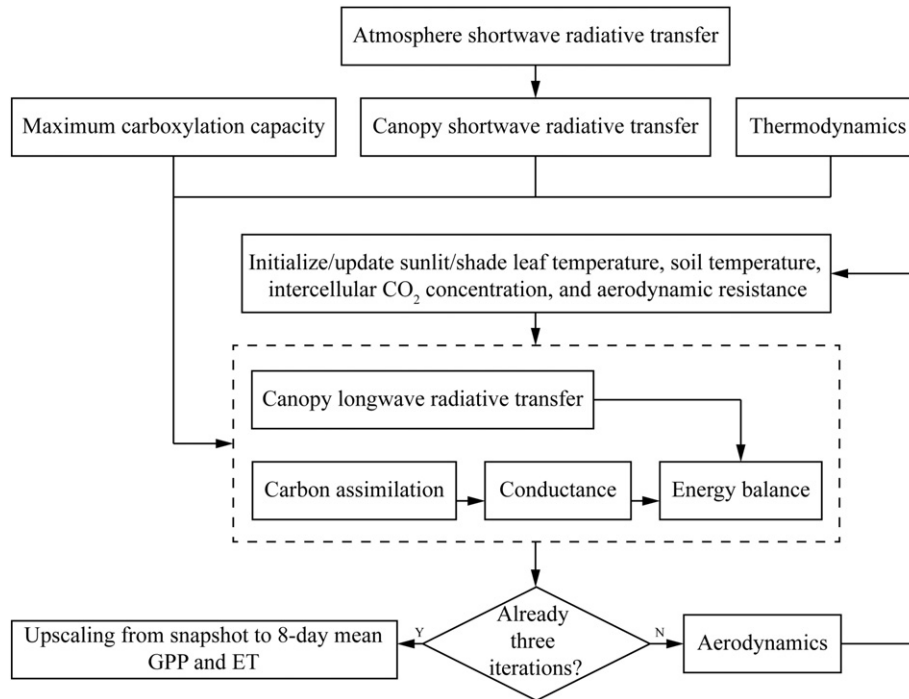


Fig. 1. Algorithm flowchart of BESS products.

time-series analysis approach to mitigate cloud contamination. Six datasets from MCD43B3 albedo product (Román et al., 2009), were used in atmosphere (black/white sky shortwave albedo) and canopy (black/white sky visible/near infrared albedo) radiative transfer modules. The Orbiting Carbon Observatory-2 (OCO-2) Lite Version-7 XCO₂ product in 2015 (oco2.gesdisc.eosdis.nasa.gov) and the National Oceanic and Atmospheric Administration (NOAA) Annual Mean Global Carbon Dioxide Growth Rates data (www.esrl.noaa.gov/gmd/ccgg/trends/) were merged to generate spatially-temporally varying ambient CO₂ concentration maps. Global clumping index map derived from MODIS (He et al., 2012), global forest canopy height product from the Geoscience Laser Altimeter System aboard Ice, Cloud, and land Elevation Satellite (ICESat/GLAS) (Simard et al., 2011), and Shuttle Radar Topography Mission (STRM) global 30 arc-second elevation product (Jarvis et al., 2008), were used for the separation of sunlit/shade canopy, calculation of aerodynamic resistance, and the consideration of altitude effect on incoming radiation, respectively. We used air temperature and dew point temperature derived from MOD07_L2 product, which were gap-filled and harmonized using ERA Interim Reanalysis data (www.apps.ecmwf.int/datasets/data/interim-full-daily). NCEP/NCAR Reanalysis wind speed data (www.esrl.noaa.gov/psd/data/gridded/) were used in the aerodynamic module. By using the global C3 and C4 distribution map (Still, 2003), the carbon-water-coupled module was performed for the C3 and C4 species separately in a pixel, and the sum of relative proportion of C3 and C4 for the pixel determined the GPP and ET at the pixel. Global climate classification map (Peel et al., 2006), along with the synthesized land cover map, were used to build a PFT-dependent LUT for V_{max}^{25C} (Table A1). Compared to the previous version (Ryu et al., 2011), the CO₂ concentration, canopy height, and elevation data were newly-incorporated, and the clumping index data were updated with finer resolution. In addition, reprojection algorithm, LAI filtering algorithm, and temperature filling algorithm were improved, and the CO₂ concentration maps were made and applied (Appendix A).

2.2. MPI-BGC GPP and ET products

MPI-BGC GPP and ET products were provided in monthly composite and in 0.5° resolution from 1982 to 2011 (Jung et al., 2011). The

products utilized a model tree ensemble to establish a statistical relationship between FLUXNET observed fluxes and 29 explanatory variables, which was mainly derived from a harmonized satellite-derived fraction of absorbed photosynthetic active radiation (fPAR) product and CRU temperature and precipitation datasets. As a proxy for FLUXNET observations, it has been commonly considered as the benchmark or reference in global carbon and water cycles studies (Anav et al., 2015; Huang et al., 2015).

2.3. MODIS GPP and ET products

MOD17A2 GPP (Collection 5.5) and MOD16A2 ET (Version 1.05) products were separately provided in 8-day composite and 1 km resolution from 2000 to 2014. MOD17A2 GPP product adopted a light use efficiency (LUE) model (Monteith, 1972; Running et al., 2004; Zhao et al., 2005). It assumed GPP was proportionally related to APAR under ideal conditions. The maximum LUE was based on a PFT-dependent look-up table, fPAR was from MOD15A2, and PAR was computed from the shortwave radiation provided by DAO. Two simple linear scalars were incorporated to account for temperature and water stress, using DAO daily minimum temperature and vapor pressure deficit, respectively. MOD16A2 product adopted a linear form of the Penman-Monteith equation to estimate ET (Mu et al., 2007, 2011). Canopy ET and soil evaporation were computed separately, using MOD15A2 fPAR as a proxy of the fraction of vegetation cover. Net radiation was computed from the energy balance using DAO shortwave radiation, MCD43B3 albedo, and DAO temperature for both air and surface. Surface conductance was assumed to be linearly related to LAI, and, like MOD17A2, was corrected by temperature and water stress scalars.

2.4. FLUXNET GPP and ET observations

The FLUXNET2015 Dataset included data collected at sites from multiple regional flux networks between 1991 and 2014 (www.fluxnet.fluxdata.org/data/), with several improvements to the data quality control protocols and the data processing pipeline compared to its predecessor LaThuille 2007 dataset. A total of 113 Tier-1 sites under fair-use data policy were included in the FLUXNET2015 v1.1 dataset (Table

A2). These sites covered a wide range of PFTs across arctic to tropical climate zones over all continents except for the Antarctica (Fig. 2). We used GPP flux data from nighttime partitioning of net ecosystem CO₂ exchange (NEE) and latent heat (LE) flux data with energy balance closure correction when available. Standard temporal aggregations were provided at daily, monthly and yearly time steps. Quality flags, NEE_VUT_REF_QC and LE_F_MDS_QC, were associated with each temporal aggregation, indicating percentage of measured and good quality gap-filled data for each day/month/year for NEE and LE, respectively.

2.5. Evaluation of BESS products

At site level, evaluation of BESS GPP and ET products was conducted in terms of overall accuracy, spatial variability, seasonal variability, and interannual variability, by comparing with FLUXNET data. Only 1-km resolution pixels containing the flux tower were used for comparison. MODIS products having the same spatial and temporal resolution with BESS were also involved in the comparison. MPI-BGC products, trained from FLUXNET data and provided in coarse resolution (0.5°), were not taken into consideration at site level.

For overall accuracy, BESS and MODIS 8-day mean GPP and ET were directly compared to the FLUXNET data. At this point, daily FLUXNET data with quality flag > 0.75 were averaged to 8-day mean. Such criteria led to 29,797 valid data over 113 sites (742 site years) and 22,531 valid data over 75 sites (547 site years) involved in the comparison for GPP and ET, respectively. Coefficient of determination (R²), root mean squared error (RMSE) and bias were used to quantify overall accuracy of BESS and MODIS 8-day mean GPP and ET products.

For spatial variability, BESS and MODIS mean annual sum GPP and ET were compared to the FLUXNET data. At this point, yearly FLUXNET data with quality flag > 0.75 were averaged to mean annual sum site by site, and BESS and MODIS mean annual sum data were calculated over the site-years corresponding to available FLUXNET data. Such criteria led to 99 and 63 sites involved in the comparison for GPP and ET, respectively. We defined spatial variability as the standard deviation of mean annual sum data over the sites, and it was calculated PFT by PFT for FLUXNET, BESS, and MODIS, respectively. We also calculated R² between BESS/MODIS and FLUXNET for each PFT to quantify the proportion of spatial variability in FLUXNET data explained by BESS and MODIS. Another metric, normalized root mean squared error (NRMSE) (Keenan et al., 2012), was further used to quantify mismatch

between BESS/MODIS and FLUXNET. It was defined as RMSE normalized by the magnitude of FLUXNET spatial variability:

$$\text{NRMSE} = \frac{\sqrt{\frac{\sum_{i=1}^n (\delta_{i,\text{FLUXNET}} - \delta_{i,\text{satellite}})^2}{n}}}{\sqrt{\frac{\sum_{i=1}^n (\delta_{i,\text{FLUXNET}} - \bar{\delta}_{\text{FLUXNET}})^2}{n}}} \quad (1)$$

where n refers to the number of sites within a PFT, δ_i is spatial anomaly defined as the mean annual sum GPP or ET at the i th site subtracted by the average value over the n sites, the subscripts FLUXNET and satellite further indicated that the data were from FLUXNET and satellite (BESS or MODIS), respectively, and symbol $\bar{}$ means average over n sites.

For seasonal variability, BESS and MODIS mean monthly GPP and ET were compared to FLUXNET data. At this point, monthly FLUXNET data with quality flag > 0.75 were averaged over available years site by site, and BESS and MODIS mean monthly data were calculated over site-years corresponding to available FLUXNET data. Only sites having mean monthly data over all 12 months were used. Such criteria led to 92 and 67 sites involved in the comparison for GPP and ET, respectively. We defined seasonal variability as the standard deviation of mean monthly data over 12 months, and it was calculated site by site and subsequently averaged PFT by PFT for FLUXNET, BESS, and MODIS, respectively. We also calculated R² between BESS/MODIS and FLUXNET for each site to quantify the proportion of seasonal variability in FLUXNET data explained by BESS and MODIS. We further calculated NRMSE site by site with quantities in Eq (1) changed, where $n = 12$ refers to the number of months, δ_i is seasonal anomaly defined as the mean monthly GPP or ET at the i th month subtracted by the average value over the n months, and symbol $\bar{}$ means average over n months.

For interannual variability, BESS and MODIS annual sum GPP and ET were compared to FLUXNET data. Only sites having at least three yearly data with quality flag > 0.75 were used. Such criteria led to 60 and 47 sites involved in the comparison for GPP and ET, respectively. We defined interannual variability as the standard deviation of annual sum data over available years, and it was calculated site by site and subsequently averaged PFT by PFT for FLUXNET, BESS, and MODIS, respectively. We also calculated R² between BESS/MODIS and FLUXNET for each site to quantify the proportion of interannual variability in FLUXNET data explained by BESS and MODIS. We further calculated NRMSE site

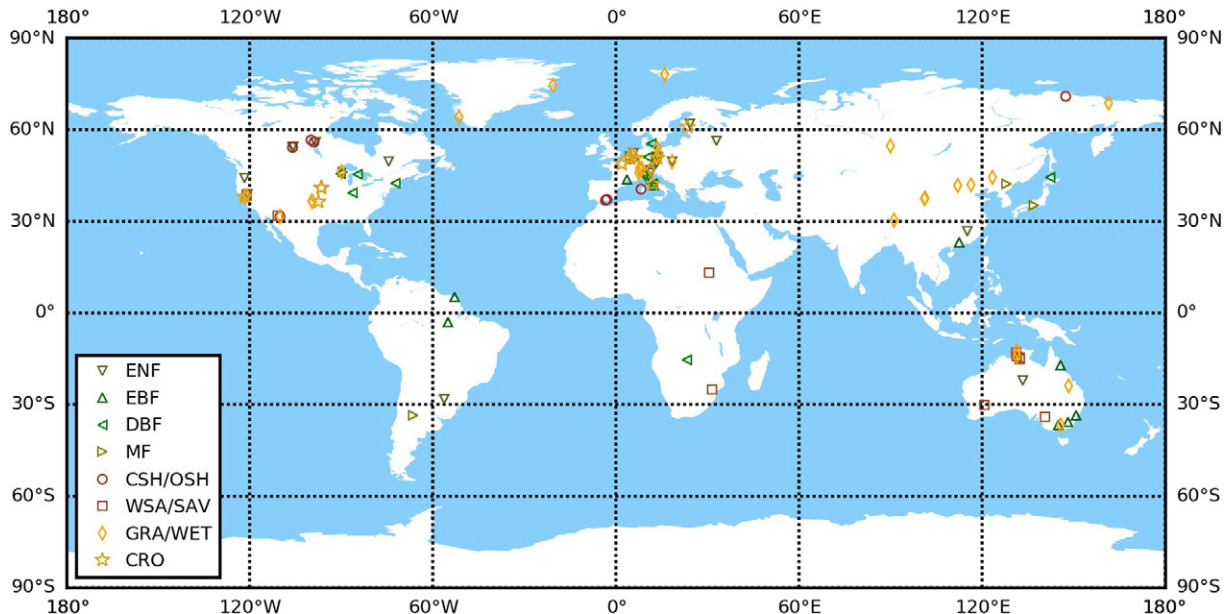


Fig. 2. Distribution of 113 sites in FLUXNET2015 v1.1 Tier 1 dataset.

by site with quantities in Eq (1) changed, where $n \geq 3$ refers to the number of available years, δ_i is annual anomaly defined as the annual sum GPP or ET at the i th year subtracted by the average value over the n years, and symbol $\bar{}$ means average over n years.

At global level, to investigate the spatiotemporal consistency and discrepancy between BESS and the other two products, i.e., MPI-BGC and MODIS, evaluations were conducted in terms of global mean total values, global annual anomalies, mean annual sum pattern, interannual variability pattern, and trend pattern of GPP and ET. All intercomparison were made between 2001 and 2011, overlapped time span of the three products. The year 2000 was excluded from BESS because official MODIS atmosphere and land products were not available in the first two months.

For global mean total values of GPP and ET, associated uncertainties were also quantified for BESS and MODIS. We averaged mean annual sum GPP and ET over all sites within each PFT, for FLUXNET, BESS, and MODIS, respectively (Tables 2 and 3). Relative RMSE values of these PFT-averaged mean annual sum GPP and ET between FLUXNET and BESS or MODIS were computed and considered as relative uncertainties for BESS and MODIS GPP and ET products. The corresponding absolute uncertainties were obtained by multiplying the relative uncertainties with global mean total values of GPP and ET.

For global annual anomalies of GPP and ET, we calculated them as global annual total values subtracting by global mean total values between 2001 and 2011. We defined interannual variability as the standard deviation of annual sum data over this overlapped time span. A Mann-Kendall test was used to examine the significance of trends. We further calculated correlation coefficients of time series between the three products to investigate their temporal consistency.

All map-to-map intercomparison were made in monthly-composite and 0.5° resolution between 2001 and 2011, considering the spatiotemporal resolution and time span of the three products. At this point, both BESS and MODIS data were aggregated by averaging 1-km resolution data in each 0.5° grid. The land mask was constrained by the spatial intersection of the three datasets to facilitate map-to-map analysis. To investigate their spatial consistency, we calculated correlation coefficients of mean annual sum maps, interannual variability maps, and trend maps between the three products.

3. Results

3.1. Direct evaluation against FLUXNET site observations

3.1.1. Overall accuracy

Overall, both BESS GPP and ET 8-day composite 1-km resolution products agreed with FLUXNET observations (Table 1), with 67% of GPP and 62% of ET variations explained by BESS. The average RMSE values for BESS were $2.58 \text{ gC m}^{-2} \text{ d}^{-1}$ and 0.78 mm d^{-1} for GPP and ET, respectively. In case of GPP, the largest RMSE was found in croplands

($3.86 \text{ gC m}^{-2} \text{ d}^{-1}$), followed by evergreen broadleaved forest ($2.97 \text{ gC m}^{-2} \text{ d}^{-1}$), while the largest bias was found in evergreen needleleaf forest ($-1.28 \text{ gC m}^{-2} \text{ d}^{-1}$), followed by croplands ($-1.21 \text{ gC m}^{-2} \text{ d}^{-1}$). In case of ET, both evergreen broadleaved forest and close shrublands/open shrublands showed relatively large RMSE values (around 1.12 mm d^{-1}), accompanied by large bias values (0.40 mm d^{-1}). MODIS had similar accuracy statistics, which explained 59% GPP variations and 52% ET variations. The average RMSE values for MODIS were $2.86 \text{ gC m}^{-2} \text{ d}^{-1}$ and 0.86 mm d^{-1} for GPP and ET, respectively. Croplands showed the largest GPP RMSE ($4.80 \text{ gC m}^{-2} \text{ d}^{-1}$) and evergreen broadleaved forest showed the largest ET RMSE (1.26 mm d^{-1}). MODIS also exhibited slight underestimation in GPP ($-0.73 \text{ gC m}^{-2} \text{ d}^{-1}$), especially in croplands ($-1.34 \text{ gC m}^{-2} \text{ d}^{-1}$) and evergreen needleleaf forest ($-0.91 \text{ gC m}^{-2} \text{ d}^{-1}$), and overestimation in ET (0.14 mm d^{-1}), especially in evergreen broadleaved forest (0.87 mm d^{-1}).

3.1.2. Spatial variability

The FLUXNET spatial variability were $668 \text{ gC m}^{-2} \text{ y}^{-1}$ (53%) and 224 mm y^{-1} (39%) for GPP and ET, over 99 and 63 sites, respectively (Tables 2 and 3). BESS tended to slightly underestimate spatial variability for both GPP and ET, in particular, by $>15\%$ in evergreen broadleaf forest and grasslands/permanent wetlands. About 52% of spatial variability in FLUXNET GPP and ET were explained by BESS, and overall NRMSE of BESS GPP and ET were around 70%. These statistics were similar to MODIS. In case of GPP, both BESS and MODIS had relatively large NRMSE values in deciduous broadleaved forest, mixed forest, and croplands. In case of ET, relatively large NRMSE values were found in deciduous broadleaved forest, mixed forest, and close shrublands/open shrublands.

3.1.3. Seasonal variability

BESS had consistent seasonal trajectory with FLUXNET observations for both GPP and ET (Tables 4 and 5). On average, BESS explained about 85% seasonal variations, with NRMSE about 50%. Relatively high R^2 values (>0.80) were achieved in most of PFTs. The lowest R^2 values of BESS were yielded in evergreen broadleaf forest (0.64 for GPP and 0.60 for ET), corresponding to the lowest observed seasonal variability (21% for GPP and 51% for ET). Relative low R^2 values were also found in woody savanna/savanna (0.76) for BESS GPP and in close shrublands/open shrublands (0.64) for BESS ET. Similar to R^2 , NRMSE values were higher (around 100%) in evergreen broadleaf forest for both BESS GPP and ET. Except for evergreen broadleaf forest, all the other PFTs exhibited NRMSE values smaller than 60% in case of GPP, while a large NRMSE (135%) was observed in close shrublands/open shrublands for ET. When compared to MODIS, BESS GPP and ET generally showed higher R^2 values and lower NRMSE values, yet they were not significantly different as the 95% confidence interval overlapped each

Table 1
 R^2 , RMSE, and bias of BESS and MODIS 8-day composite 1-km resolution GPP and ET products evaluated against FLUXNET observations. The units of RMSE and bias are $\text{gC m}^{-2} \text{ d}^{-1}$ and mm d^{-1} for GPP and ET, respectively. Bold style indicates a higher R^2 or a lower RMSE. PFTs: evergreen needle leaved forest (ENF), evergreen broadleaved forest (EBF), deciduous broadleaved forest (DBF), mixed forest (MF), close shrublands (CSH), open shrublands (OSH), woody savannas (WSA), savannas (SAV), grasslands (GRA), permanent wetlands (WET), and croplands (CRO).

PFT	BESS GPP			MODIS GPP			BESS ET			MODIS ET		
	R^2	RMSE	Bias									
ENF	0.73	2.37	-1.28	0.74	2.12	-0.91	0.64	0.70	-0.09	0.58	0.74	0.11
EBF	0.25	2.97	-0.78	0.25	2.96	-0.23	0.43	1.12	0.40	0.58	1.26	0.87
DBF	0.72	2.59	-0.09	0.68	2.97	-0.71	0.77	0.84	0.39	0.67	0.91	0.50
MF	0.67	2.31	-0.83	0.65	2.30	-0.72	0.83	0.66	0.39	0.70	0.97	0.67
CSH/OSH	0.77	1.37	0.68	0.68	1.56	0.82	0.32	1.13	0.40	0.33	0.66	0.00
WSA/SAV	0.52	1.69	-0.43	0.49	1.79	-0.54	0.54	0.75	0.20	0.48	0.80	-0.25
GRA/WET	0.71	2.24	-0.45	0.64	2.59	-0.78	0.63	0.74	0.11	0.50	0.88	0.12
CRO	0.74	3.86	-1.21	0.49	4.80	-1.34	0.74	0.70	-0.18	0.58	0.88	-0.17
Overall	0.67	2.58	-0.68	0.59	2.86	-0.73	0.62	0.78	0.10	0.52	0.86	0.14

Table 2

Performance of BESS and MODIS GPP products in terms of spatial variability. Numbers in parenthesis are spatial variability normalized by PFT-averaged mean annual sum GPP. Bold style indicates a higher R^2 or a lower NRMSE (see Eq. (1)). PFT full names are referred to Table 1.

PFT	Sites	Mean annual sum ($\text{gC m}^{-2} \text{y}^{-1}$)			Spatial variability ($\text{gC m}^{-2} \text{y}^{-1}$)			R^2		NRMSE	
		FLUXNET	BESS	MODIS	FLUXNET	BESS	MODIS	BESS	MODIS	BESS	MODIS
ENF	20	1377	1050	1173	627 (45%)	373 (35%)	417 (35%)	0.80	0.80	53%	50%
EBF	9	1980	1907	2087	829 (41%)	291 (15%)	570 (27%)	0.63	0.37	75%	80%
DBF	14	1504	1442	1319	299 (19%)	520 (36%)	306 (23%)	0.05	0.09	180%	120%
MF	6	1639	1172	1296	425 (25%)	362 (30%)	267 (20%)	0.47	0.04	170%	128%
CSH/OSH	5	498	758	869	329 (66%)	490 (64%)	461 (53%)	0.99	0.86	50%	60%
WSA/SAV	10	797	624	638	431 (54%)	319 (51%)	245 (38%)	0.35	0.54	81%	69%
GRA/WET	25	1033	955	842	661 (64%)	468 (49%)	442 (52%)	0.70	0.70	56%	57%
CRO	10	1202	929	933	375 (31%)	139 (15%)	234 (25%)	0.32	0.02	84%	124%
Overall	99	1258	1097	1107	668 (53%)	524 (47%)	544 (49%)	0.52	0.57	69%	65%

other. The only significant difference appeared in croplands for GPP, where BESS yielded 16% lower NRMSE than MODIS.

3.1.4. Interannual variability

Both BESS and MODIS tended to underestimate interannual variability of GPP and ET. FLUXNET showed GPP interannual variability of 15% over 60 sites and ET interannual variability of 13% over 47 sites, while BESS and MODIS only yielded 5–8%. BESS and MODIS GPP were only able to explain around 35% of the interannual variability in site observations, and the proportion was even lower for ET which was only around 25%. The overall NRMSE values were above 100% for both BESS and MODIS for both GPP and ET. With regard to PFT, BESS GPP and ET products showed the lowest NRMSE for woody savannas/savannas (78% for GPP and 84% for ET) which had the largest observed interannual variability (26% for GPP and 23% for ET). Although very high NRMSE values appeared in close shrublands/open shrublands for GPP (269%) and in evergreen broadleaf forest for ET (203%), their 95% confidence interval were even larger. Similar performance appeared for the other PFTs, with mean NRMSE values ranging from 78% to 110%. There was no significant difference between BESS and MODIS. In fact, BESS and MODIS time series were more similar with each other, than compared to FLUXNET. Examples were shown in Figs. 3 and 4, in which only sites with at least 10 years annual data were included. At most sites, BESS annual anomalies of GPP and ET matched MODIS but both exhibited less fluctuation than FLUXNET. In addition, seven and eight sites showed significant ($p < 0.05$) trends for GPP and ET, respectively, but none of them were detected by BESS or MODIS.

3.2. Global intercomparison with MPI-BGC and MODIS

3.2.1. Global total GPP and ET

The mean annual global total GPP and ET derived from BESS between 2001 and 2011 were $122 \pm 25 \text{ PgC y}^{-1}$ and $65 \times 10^3 \pm 11 \times 10^3 \text{ km}^3 \text{ y}^{-1}$, respectively. These values were almost the same as that of MPI-BGC (120 PgC y^{-1} for GPP and $65 \times 10^3 \text{ km}^3 \text{ y}^{-1}$ for ET), and higher than that of MODIS ($110 \pm 23 \text{ PgC y}^{-1}$ for GPP and

$62 \times 10^3 \pm 13 \times 10^3 \text{ km}^3 \text{ y}^{-1}$ for ET), with uncertainty ranges overlapped with each other.

3.2.2. Global annual anomalies of GPP and ET

The annual anomalies in GPP and ET for BESS, MPI-BGC and MODIS were shown in Fig. 5. For GPP (Fig. 5a), the interannual variability of BESS (1.13 PgC y^{-1}) tended to fall in between that of MPI-BGC (1.69 PgC y^{-1}) and MODIS (0.77 PgC y^{-1}). The temporal pattern of BESS was more similar to MPI-BGC ($r = 0.65, p < 0.05$) than to MODIS ($r = 0.56, p < 0.1$). Four valleys were found in BESS GPP annual anomaly, i.e., 2002, 2005, 2009 and 2012, consistent with either MPI-BGC or MODIS. Both BESS and MPI-BGC displayed increasing GPP trends between 2001 and 2011, with slopes of 0.27 PgC y^{-2} ($p < 0.05$) and 0.35 PgC y^{-2} ($p < 0.1$), respectively. With regards to ET (Fig. 5b), the interannual variability followed BESS ($0.51 \times 10^3 \text{ km}^3 \text{ y}^{-1}$) < MPI-BGC ($0.63 \times 10^3 \text{ km}^3 \text{ y}^{-1}$) < MODIS ($0.87 \times 10^3 \text{ km}^3 \text{ y}^{-1}$). There was no significant correlation between BESS and MPI-BGC ($p > 0.1$), and between BESS and MODIS ($p > 0.1$), but the three products illustrated similar temporal patterns from 2007 to 2011. During the period of 2001–2011, only MODIS displayed an increasing ET trend by $0.22 \times 10^3 \text{ km}^3 \text{ y}^{-2}$ ($p < 0.01$), whereas BESS and MPI-BGC did not show significant trends. When extended to 2015, BESS GPP had a slope of 0.26 PgC y^{-2} ($p < 0.001$) and BESS ET had a slope of $-0.06 \times 10^3 \text{ km}^3 \text{ y}^{-1}$ ($p < 0.1$).

3.2.3. Patterns of mean annual sum GPP and ET

In general, large BESS mean annual GPP and ET values appeared in densely vegetated areas (Fig. 6). The equatorial regions where the evergreen broadleaf forest dominates had the highest mean annual GPP and ET values, up to $3500 \text{ gC m}^{-2} \text{y}^{-1}$ and 1500 mm y^{-1} , respectively. Five peaks of GPP and ET values appeared on the southeast side of all continents between latitudes 25° and 40° : southeastern China, southeastern United States, southeastern Brazil, southeastern Africa, and southeastern Australia, corresponding to humid subtropical climate. Another hotspot was identified in the boreal regions (60° N), which covered a large area over Russia, Europe, and Canada. Dry regions in the center

Table 3

Performance of BESS and MODIS ET products in terms of spatial variability. Numbers in parenthesis are spatial variability normalized by PFT-averaged mean annual sum ET. Bold style indicates a higher R^2 or a lower NRMSE (see Eq. (1)). PFT full names are referred to Table 1.

PFT	Sites	Mean annual sum (mm y^{-1})			Spatial variability (mm y^{-1})			R^2		NRMSE	
		FLUXNET	BESS	MODIS	FLUXNET	BESS	MODIS	BESS	MODIS	BESS	MODIS
ENF	14	531	440	504	143 (26%)	122 (27%)	118 (23%)	0.47	0.35	74%	83%
EBF	2	919	884	1076	405 (44%)	231 (26%)	312 (28%)	1.00	1.00	42%	23%
DBF	9	675	604	596	133 (19%)	141 (23%)	129 (21%)	0.11	0.02	119%	148%
MF	3	444	464	588	27 (6%)	12 (2%)	65 (11%)	0.31	0.67	83%	324%
CSH/OSH	3	354	503	344	94 (26%)	279 (55%)	186 (54%)	1.00	0.82	195%	114%
WSA/SAV	7	473	466	297	142 (30%)	161 (34%)	184 (61%)	0.83	0.84	46%	54%
GRA/WET	15	567	487	506	286 (50%)	141 (28%)	209 (41%)	0.73	0.44	63%	74%
CRO	10	666	469	474	173 (25%)	105 (22%)	57 (12%)	0.60	0.18	65%	90%
Overall	63	575	501	505	224 (39%)	168 (33%)	208 (41%)	0.51	0.41	70%	81%

Table 4
Performance of BESS and MODIS GPP products in terms of seasonal variability. Numbers in parenthesis are seasonal variability normalized by mean GPP over 12 months. All variability, R^2 and NRMSE values are average over sites within each PFT, and numbers after \pm symbol are 95% confidence interval. Bold style indicates a higher R^2 or a lower NRMSE (see Eq. (1)). PFT full names are referred to Table 1.

PFT	Sites	Seasonal variability ($\text{gC m}^{-2} \text{mon}^{-1}$)			R^2		NRMSE	
		FLUXNET	BESS	MODIS	BESS	MODIS	BESS	MODIS
ENF	18	80 (78%)	69 (82%)	75 (80%)	0.92 \pm 0.05	0.89 \pm 0.12	34% \pm 5%	36% \pm 11%
EBF	7	31 (21%)	46 (29%)	42 (24%)	0.64 \pm 0.19	0.64 \pm 0.09	113% \pm 45%	121% \pm 61%
DBF	13	121 (93%)	98 (81%)	79 (71%)	0.83 \pm 0.15	0.82 \pm 0.08	43% \pm 14%	49% \pm 8%
MF	5	89 (69%)	77 (77%)	73 (65%)	0.90 \pm 0.16	0.85 \pm 0.11	39% \pm 21%	44% \pm 13%
CSH/OSH	5	37 (116%)	48 (81%)	51 (74%)	0.88 \pm 0.13	0.64 \pm 0.35	58% \pm 19%	81% \pm 19%
WSA/SAV	10	43 (68%)	30 (53%)	25 (43%)	0.76 \pm 0.12	0.51 \pm 0.25	58% \pm 12%	75% \pm 22%
GRA/WET	24	76 (116%)	69 (87%)	56 (79%)	0.85 \pm 0.09	0.78 \pm 0.09	51% \pm 13%	51% \pm 10%
CRO	10	121 (117%)	74 (97%)	61 (81%)	0.89 \pm 0.09	0.80 \pm 0.08	46% \pm 6%	62% \pm 9%
Overall	92	80 (90%)	67 (77%)	60 (69%)	0.84 \pm 0.04	0.77 \pm 0.08	51% \pm 6%	58% \pm 9%

of Eurasia and locations at the southwest side of all continents between latitudes 25° and 40° had very low GPP and ET values, as well as the Arctic regions.

Overall, BESS mean annual GPP and ET agreed well with MPI-BGC, indicated by a high R^2 (0.93 for GPP and 0.90 for ET) and a small RMSE ($229 \text{ gC m}^{-2} \text{ y}^{-1}$ for GPP and 118 mm y^{-1} for ET) (Table 9). A

Table 5
Performance of BESS and MODIS ET products in terms of seasonal variability. Numbers in parenthesis are seasonal variability normalized by mean ET over 12 months. All variability, R^2 and NRMSE values are average over sites within each PFT, and numbers after \pm symbol are 95% confidence interval. Bold style indicates a higher R^2 or a lower NRMSE (see Eq. (1)). PFT full names are referred to Table 1.

PFT	Sites	Seasonal variability (mm mon^{-1})			R^2		NRMSE	
		FLUXNET	BESS	MODIS	BESS	MODIS	BESS	MODIS
ENF	13	30 (75%)	29 (87%)	28 (69%)	0.94 \pm 0.05	0.91 \pm 0.11	28% \pm 11%	29% \pm 11%
EBF	4	21 (51%)	27 (45%)	27 (33%)	0.60 \pm 0.22	0.70 \pm 0.26	95% \pm 44%	93% \pm 101%
DBF	8	43 (87%)	38 (76%)	31 (62%)	0.94 \pm 0.04	0.85 \pm 0.17	29% \pm 10%	40% \pm 17%
MF	4	28 (80%)	31 (78%)	28 (63%)	0.92 \pm 0.13	0.89 \pm 0.21	31% \pm 29%	38% \pm 32%
CSH/OSH	4	19 (68%)	23 (60%)	12 (47%)	0.64 \pm 0.60	0.48 \pm 0.64	135% \pm 81%	90% \pm 79%
WSA/SAV	8	27 (63%)	17 (40%)	17 (58%)	0.84 \pm 0.08	0.70 \pm 0.18	51% \pm 10%	77% \pm 27%
GRA/WET	15	30 (71%)	28 (71%)	24 (55%)	0.84 \pm 0.13	0.79 \pm 0.14	37% \pm 13%	55% \pm 16%
CRO	11	39 (73%)	28 (75%)	23 (58%)	0.91 \pm 0.08	0.91 \pm 0.06	40% \pm 13%	49% \pm 10%
Overall	67	31 (72%)	28 (70%)	24 (58%)	0.86 \pm 0.05	0.81 \pm 0.06	45% \pm 13%	53% \pm 10%

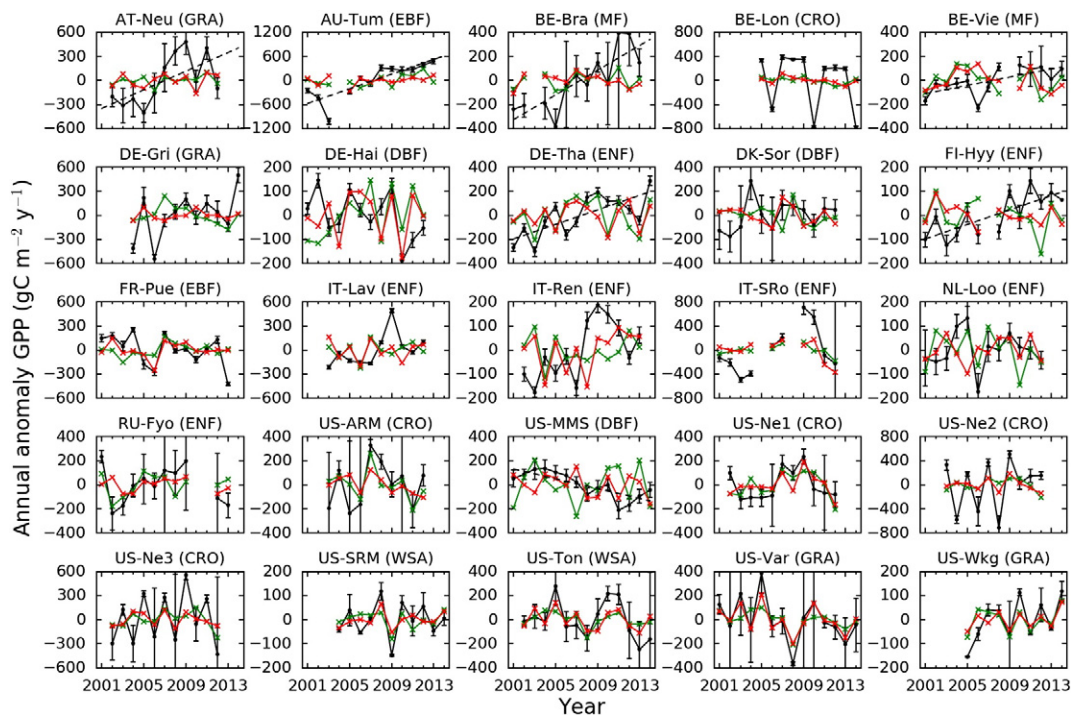


Fig. 3. Comparison of annual anomaly GPP of BESS (red lines), MODIS (green lines), and FLUXNET (black lines) over 25 sites. Error bars with FLUXNET refer to annual uncertainties reported in the FLUXNET2015 dataset multiplied by two corresponding to a 95% confidence interval (Keenan et al., 2012). Dash lines indicate significant trends ($p < 0.05$).

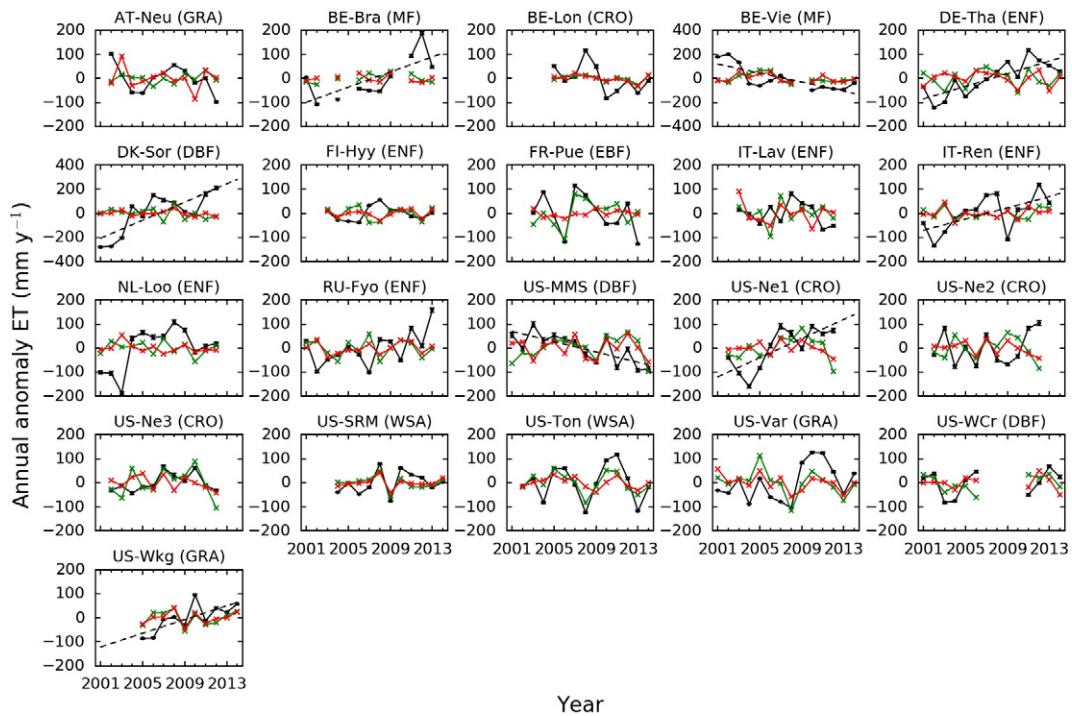


Fig. 4. Comparison of annual anomaly ET of BESS (red lines), MODIS (green lines), and FLUXNET (black lines) over 21 sites. Error bars with FLUXNET refer to annual uncertainties reported in the FLUXNET2015 dataset multiplied by two corresponding to a 95% confidence interval (Keenan et al., 2012). Dash lines indicate significant trends ($p < 0.05$).

consistent GPP relationship ($R^2 \geq 0.92$) was also observed between BESS and MODIS, and between MODIS and MPI-BGC, but not for ET ($R^2 \leq 0.85$). Spatially, BESS GPP showed higher values than MPI-BGC across the African tropics, and lower in Europe, southern China, and central South Africa, where BESS ET showed coherent overestimation or underestimation (Fig. 7). These could be attributed to the overestimation in woody savannas and savannas, and underestimation in evergreen needleleaf forest, deciduous broadleaf forest and mixed forest, for both GPP and ET (Table 10). Nevertheless, around 80% of the regions were characterized by BESS ~ MPI-BGC GPP deviations smaller than $400 \text{ gC m}^{-2} \text{ y}^{-1}$ and ET deviations smaller than 200 mm y^{-1} . MODIS displayed relatively larger deviations away from MPI-BGC than BESS for both GPP and ET, especially in tropical regions. However, for non-

forest regions, MODIS GPP generally showed very small differences from BESS GPP.

3.2.4. Patterns of interannual variability in GPP and ET

The global pictures for interannual variability of GPP and ET in the three products between 2001 and 2011 are shown in Fig. 8. BESS revealed similar hotspots with MPI-BGC, mainly distributed in ecological transition zones, such as northeastern Brazil, central South America, northern and eastern Australia, eastern Africa, south Central Africa, and south central United States – northeastern Mexico. The spatial correlation coefficients between BESS and MPI-BGC were 0.78 and 0.70 ($p < 0.001$) for GPP and ET, respectively. In comparison, the consistency between MODIS and MPI-BGC were relatively low. MODIS

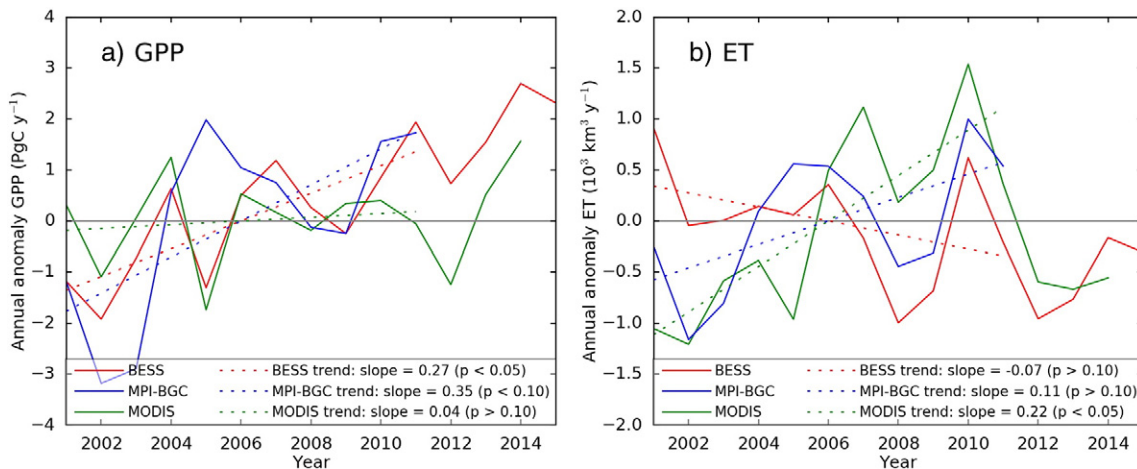


Fig. 5. Comparison of global annual anomaly of GPP (a) and ET (b) derived from the BESS, MPI-BGC and MODIS products. Trends were derived from 2001 through 2011.

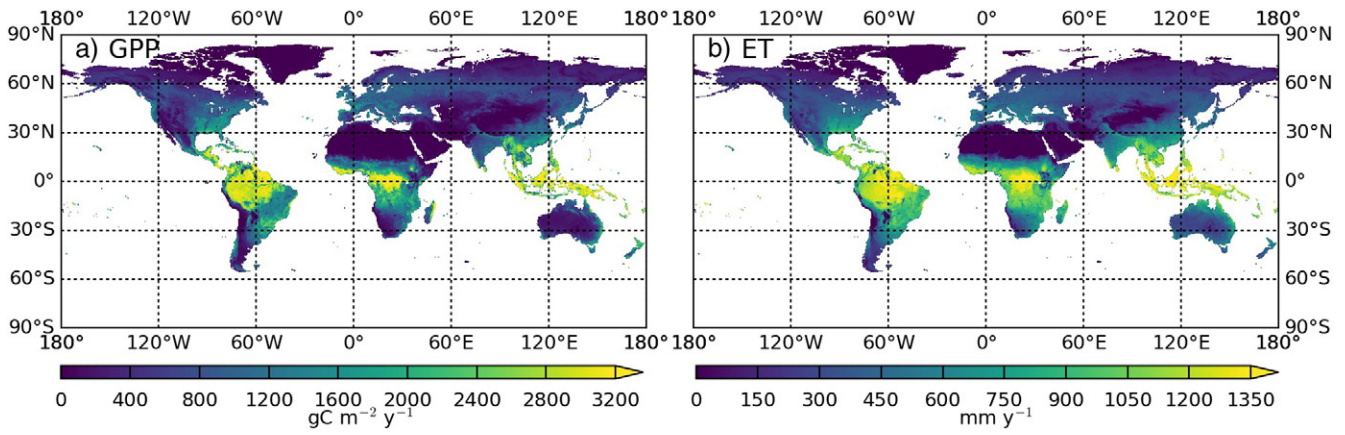


Fig. 6. The BESS global mean annual GPP and ET from 2001 to 2015.

displayed larger magnitudes than MPI-BGC, particular in tropical regions, and the spatial correlation coefficients between MODIS and MPI-BGC were only 0.50 and 0.47 ($p < 0.001$) for GPP and ET, respectively.

3.2.5. Patterns of GPP and ET trends

The geographic distributions of GPP and ET trends from 2001 to 2011 are shown in Fig. 9. In case of BESS GPP, 13% and 5% of land pixels showed significant ($p < 0.1$) increasing and decreasing

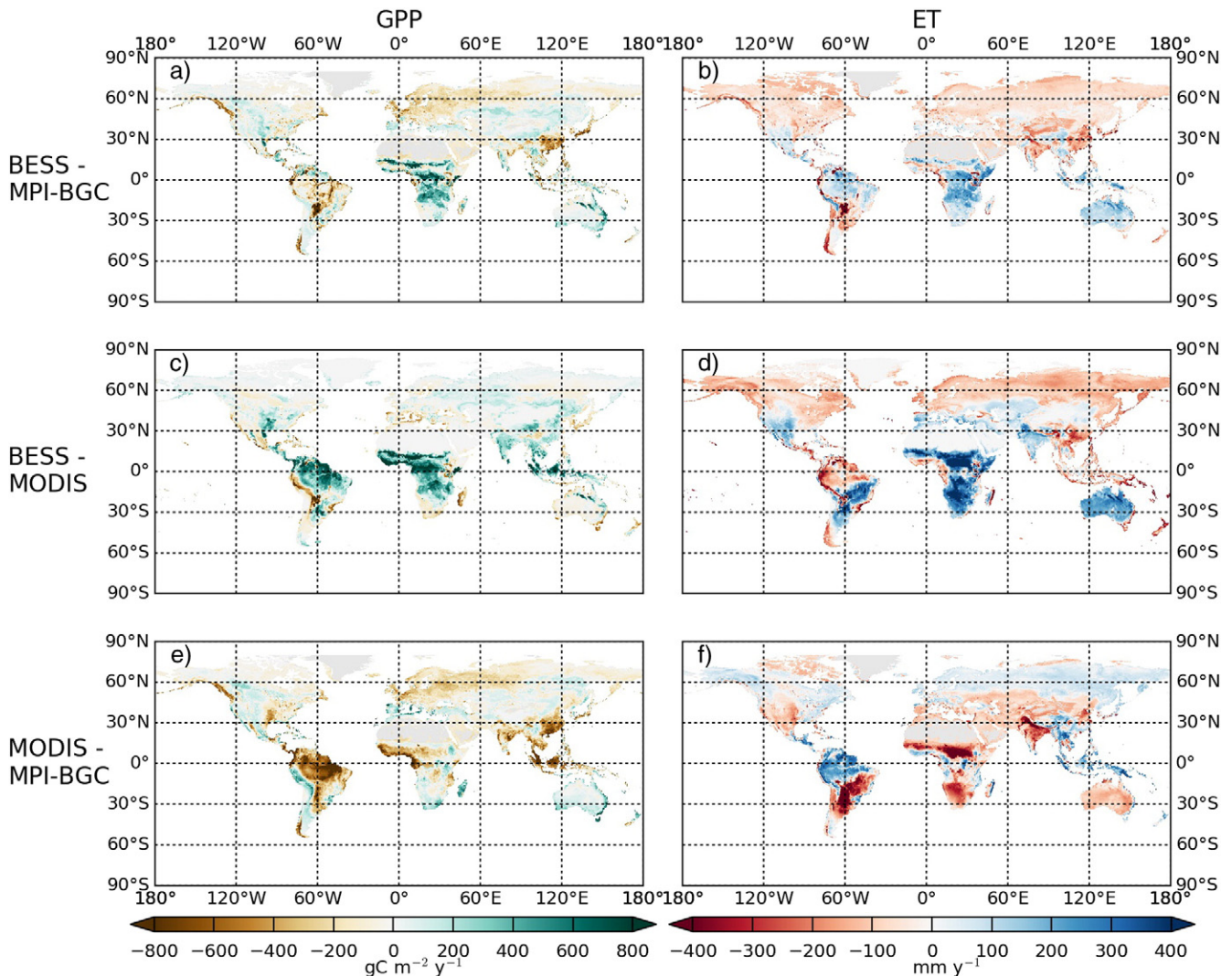


Fig. 7. Difference maps of mean annual GPP (left panel) and ET (right panel) between BESS and MPI-BGC (a and b), BESS and MODIS (c and d), and MODIS and MPI-BGC (e and f) from 2001 to 2011.

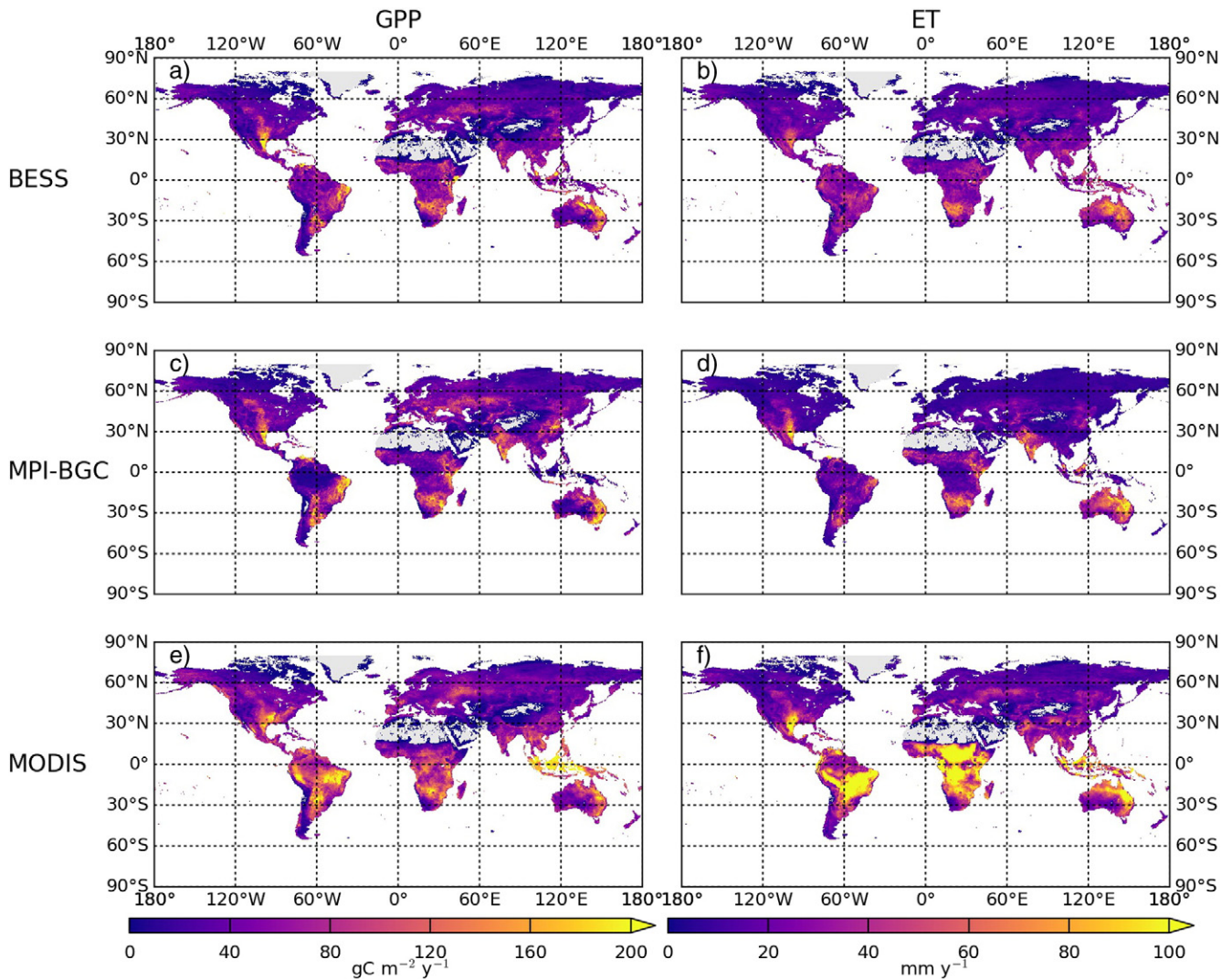


Fig. 8. Interannual variability of (a) BESS GPP, (b) BESS ET, (c) MPI-BGC GPP, (d) MPI-BGC ET, (e) MODIS GPP, and (f) MODIS ET from 2001 to 2011. Interannual variation is defined as one standard deviation over the time period.

trends, respectively. Regions with an increasing trend were mainly distributed in central Canada, northern and western Amazon, eastern Brazil, southwestern Africa, western India, eastern China, Indonesia, and northeastern Australia, while decreasing trend regions were mainly located in southeastern United States, central South America, and Kazakhstan. The spatial patterns of MPI-BGC GPP trend were overall similar to that of BESS. Irrespective of significance level, the spatial correlation coefficient between BESS and MPI-BGC was 0.73 ($p < 0.001$) over the globe, while that value between MODIS and MPI-BGC was only 0.47 ($p < 0.001$). Pronounced differences in GPP trend were apparent in Indonesia, where BESS showed positive changes, MPI-BGC had no trends, and MODIS displayed negative changes. The spatial pattern of BESS ET generally coincided with that of MPI-BGC ET as well, with a spatial correlation coefficient of 0.66 ($p < 0.001$) ignoring the significance level. Nevertheless, at the significance level of $p < 0.1$, BESS ET had less increasingly (4%) than decreasingly (11%) trendy pixels, while MPI-BGC had 13% and 5% pixels with increasing and decreasing trends, respectively. MODIS ET was visually different with the other two products in tropical regions, and the spatial correlation coefficient between MODIS and MPI-BGC was only 0.26 ($p < 0.001$).

4. Discussions

BESS, a new set of global GPP and ET products, derived from a process-based approach, demonstrated a valid overall performance at both site scale and global scale. At site scale, the overall RMSE of BESS GPP and ET products were $2.58 \text{ gC m}^{-2} \text{ d}^{-1}$ and 0.78 mm d^{-1} , respectively (Table 1), compared with FLUXNET observations over 113 sites (742 site years). These error statistics were not only similar to those of MODIS ($2.86 \text{ gC m}^{-2} \text{ d}^{-1}$ for GPP and 0.86 mm d^{-1} for ET), but also commensurate with other global GPP and ET studies. For example, $2.11 \text{ gC m}^{-2} \text{ d}^{-1}$ over 16 sites (Yebara et al., 2015), $2.20 \text{ gC m}^{-2} \text{ d}^{-1}$ over 18 sites (Yan et al., 2015), and $2.00\text{--}2.50$ over 157 sites (Yuan et al., 2014) for GPP; and 1.05 mm d^{-1} over 16 sites (Yebara et al., 2013) and 0.77 mm d^{-1} over 19 sites (Yan et al., 2012) for ET, respectively. Lower ET RMSE values were also reported by other studies, such as 0.53 mm d^{-1} over 16 sites (Fisher et al., 2008) and $0.43\text{--}0.51 \text{ mm d}^{-1}$ over 48 sites (Zhang et al., 2010). However, it is worth mentioning that differing from most of those studies, BESS is free from any calibration procedures and consequently is unlikely to be biased by unrepresentative sampling data.

At global scale, BESS agreed quite well with MPI-BGC. Considering MPI-BGC as a reference, the accuracy of BESS mean annual GPP and

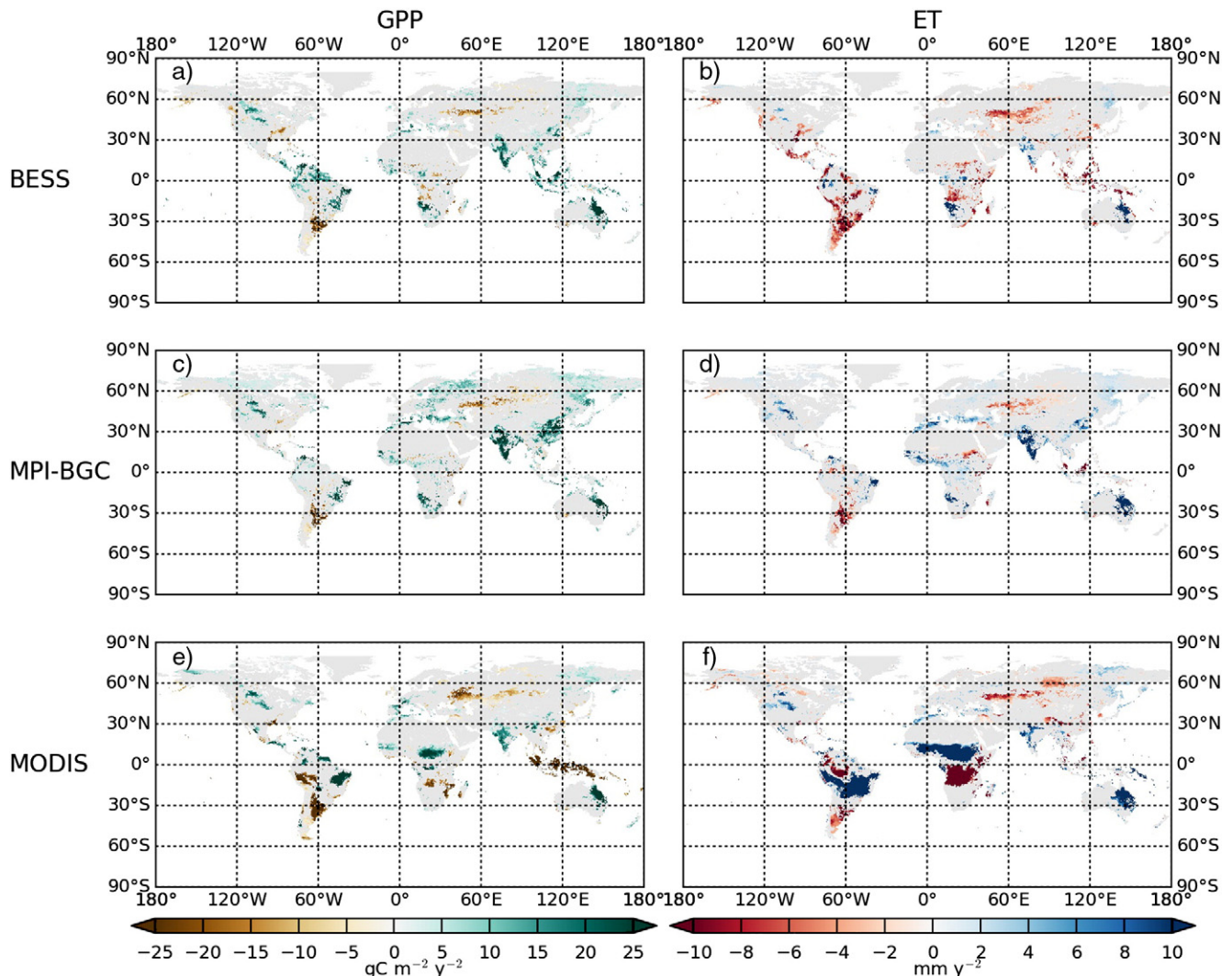


Fig. 9. Linear trends of (a) BESS GPP, (b) BESS ET, (c) MPI-BGC GPP, (d) MPI-BGC ET, (e) MODIS GPP, and (f) MODIS ET from 2001 to 2011. Nonsignificant ($p > 0.1$ according to the Mann-Kendall test) pixels are not shown.

ET were $R^2 = 0.93$ and $RMSE = 229 \text{ gC m}^{-2} \text{ y}^{-1}$; and $R^2 = 0.90$ and $RMSE = 118 \text{ mm y}^{-1}$, respectively (Table 9). These BESS–MPI-BGC R^2 values were higher than MODIS–MPI-BGC (0.92 for GPP and 0.85 for ET), and the Greenhouse Gases Observing Satellite (GOSAT) fluorescence–MPI-BGC GPP (0.80) (Frankenberg et al., 2011), as well as land surface models GPP–MPI-BGC GPP (around 0.50) (Anav et al., 2015), indicating that BESS had the best agreement with the FLUXNET upscaling product at global scale. In addition, BESS gave global total GPP and ET estimates of $122 \pm 25 \text{ PgC y}^{-1}$ and

$65 \times 10^3 \pm 11 \times 10^3 \text{ km}^3 \text{ y}^{-1}$, respectively, which were almost identical to those of MPI-BGC (Table 8). These global values followed within a reasonable range reported by other studies, such as 107 PgC y^{-1} (Yebera et al., 2015), 111 PgC y^{-1} (Yuan et al., 2010), and $120\text{--}140 \text{ PgC y}^{-1}$ (Anav et al., 2013) for GPP; and $58 \times 10^3 \text{ km}^3 \text{ y}^{-1}$ (Yan et al., 2012), $58 \times 10^3\text{--}85 \times 10^3$ (Dirmeyer et al., 2006; Jung et al., 2010), and $71 \times 10^3 \pm 7 \times 10^3 \text{ km}^3 \text{ y}^{-1}$ (Rodell et al., 2015) for ET. However, it was noted that the difference between the three products (especially between BESS and MODIS)

Table 6
Performance of BESS and MODIS GPP products in terms of interannual variability. Numbers in parenthesis are interannual variability normalized by mean GPP over available years. All variability, R^2 and NRMSE values are average over sites within each PFT, and numbers after \pm symbol are 95% confidence interval. Bold style indicates a higher R^2 or a lower NRMSE (see Eq. (1)). PFT full names are referred to Table 1.

PFT	Sites	Interannual variability ($\text{gC m}^{-2} \text{ y}^{-1}$)			R^2		NRMSE	
		FLUXNET	BESS	MODIS	BESS	MODIS	BESS	MODIS
ENF	14	144 (13%)	80 (8%)	87 (9%)	0.30 ± 0.20	0.39 ± 0.20	$104\% \pm 21\%$	$99\% \pm 20\%$
EBF	4	213 (10%)	83 (4%)	135 (5%)	0.33 ± 0.71	0.08 ± 0.12	$109\% \pm 43\%$	$126\% \pm 59\%$
DBF	8	119 (7%)	73 (4%)	88 (6%)	0.19 ± 0.18	0.09 ± 0.11	$96\% \pm 14\%$	$121\% \pm 25\%$
MF	5	116 (8%)	65 (5%)	58 (4%)	0.42 ± 0.65	0.35 ± 0.45	$97\% \pm 48\%$	$120\% \pm 23\%$
CSH/OSH	3	82 (22%)	73 (11%)	58 (10%)	0.64 ± 0.76	0.78 ± 0.55	$269\% \pm 832\%$	$256\% \pm 816\%$
WSA/SAV	5	160 (26%)	45 (8%)	68 (10%)	0.52 ± 0.13	0.54 ± 0.39	$79\% \pm 10\%$	$95\% \pm 46\%$
GRA/WET	15	181 (16%)	79 (8%)	68 (7%)	0.43 ± 0.17	0.43 ± 0.18	$78\% \pm 12\%$	$83\% \pm 19\%$
CRO	6	294 (24%)	77 (8%)	84 (11%)	0.21 ± 0.14	0.29 ± 0.32	$92\% \pm 8\%$	$90\% \pm 11\%$
Overall	60	166 (15%)	74 (7%)	80 (8%)	0.35 ± 0.11	0.36 ± 0.32	$101\% \pm 8\%$	$108\% \pm 11\%$

Table 7

Performance of BESS and MODIS ET products in terms of interannual variability. Numbers in parenthesis are interannual variability normalized by mean ET over available years. All variability, R^2 and NRMSE values are average over sites within each PFT, and numbers after \pm symbol are 95% confidence interval. Bold style indicates a higher R^2 or a lower NRMSE (see Eq. (1)). PFT full names are referred to Table 1.

PFT	Sites	Interannual variability (mm y^{-1})			R^2		NRMSE	
		FLUXNET	BESS	MODIS	BESS	MODIS	BESS	MODIS
ENF	13	67 (12%)	22 (5%)	27 (5%)	0.24 \pm 0.17	0.20 \pm 0.15	110% \pm 16%	111% \pm 17%
EBF	2	44 (7%)	20 (2%)	40 (4%)	0.50 \pm 6.16	0.43 \pm 1.96	203% \pm 329%	122% \pm 462%
DBF	6	82 (12%)	26 (4%)	40 (6%)	0.25 \pm 0.38	0.31 \pm 0.42	99% \pm 7%	94% \pm 24%
MF	3	74 (16%)	25 (5%)	32 (5%)	0.07 \pm 0.19	0.23 \pm 0.95	108% \pm 15%	91% \pm 60%
CSH/OSH	3	47 (14%)	20 (5%)	21 (11%)	0.10 \pm 0.35	0.54 \pm 0.64	101% \pm 32%	77% \pm 11%
WSA/SAV	4	118 (23%)	27 (5%)	43 (14%)	0.49 \pm 0.41	0.60 \pm 0.54	84% \pm 12%	72% \pm 22%
GRA/WET	9	76 (13%)	26 (5%)	32 (7%)	0.21 \pm 0.22	0.12 \pm 0.09	100% \pm 15%	109% \pm 13%
CRO	7	64 (10%)	25 (5%)	40 (9%)	0.14 \pm 0.13	0.23 \pm 0.16	100% \pm 11%	107% \pm 20%
Overall	47	73 (13%)	24 (5%)	33 (7%)	0.23 \pm 0.10	0.27 \pm 0.16	106% \pm 11%	101% \pm 20%

were relatively small in US, Canada, and Europe, but much larger between 30°N and 30°S (Fig. 7), where few ground truth were available (Jung et al., 2009; Sundareshwar et al., 2007).

FLUXNET observations showed large seasonal variability (90% for GPP and 72% for ET, Tables 4 and 5), middle spatial variability (53% for GPP and 39% for ET, Tables 2 and 3), and small interannual variability (15% for GPP and 13% for ET, Tables 6 and 7). Correspondingly, BESS explained a majority of seasonal variability (84% for GPP and 86% for ET, Tables 4 and 5), about half of spatial variability (52% for GPP and 51% for ET, Tables 2 and 3), and a minority of interannual variability (35% for GPP and 23% for ET, Tables 6 and 7). Similar results were also observed for MODIS (Table 2–7), and reported for MPI-BGC as well (Jung et al., 2009, 2011). In particular, the ability on capturing interannual variability was low for a wide range of remote sensing methods and land surface models (Keenan et al., 2012; Verma et al., 2014). Keenan et al. (2012) argued that process-based models could be improved by adequately modeling spring phenology, soil thaw and snowpack melting processes, and the lagged response to extreme climatic events. BESS did not explicitly consider these processes, but mainly focused on several key processes, i.e., radiative transfer, photosynthesis, conductance, and evapotranspiration. Effective and efficient parameterizations might be required to account for these missing processes. In addition, such inability might also be attributed to the input data. For example, remote sensing products highly rely on satellite LAI/fPAR datasets, but the performances of satellite LAI/fPAR products on capturing interannual variability at global and decadal scale are not well understood yet (D'Odorico et al., 2014; Garrigues et al., 2008; Ryu et al., 2012b). Additionally, incorporating satellite-derived soil moisture into carbon and water fluxes modeling, mapping and monitoring study is likely to better account for the interannual variability (Verma et al., 2015), if the accuracy and spatiotemporal resolution could be further improved (Dorigo et al., 2012). Although BESS did not explain a large portion of interannual variations at site scale, it achieved similar spatial patterns of interannual variability with MPI-BGC at global scale (Fig. 8). The latter has been proved valid in detecting spatiotemporal distribution of extreme events (Zscheischler et al., 2013, 2014), indicating BESS has potentials in similar global applications but with higher spatial resolution.

At decadal scale (2001–2011), BESS produced a significant ascending GPP trend by 0.27 PgC y^{-2} ($p < 0.05$) (Fig. 5a). MODIS did not show

any trend, and MPI-BGC displayed a trend of 0.35 PgC y^{-2} with a lower significance ($p < 0.1$). In comparison, state-of-the-art land surface models usually yield ascending trends ranging from 0.2 to 0.4 PgC y^{-2} (Anav et al., 2013, 2015), and BESS followed within this range. Furthermore, the Free-Air CO₂ Enrichment (FACE) experiment reveals that the sensitivity of net primary productivity to CO₂ fertilization effect is around $0.13\% \text{ ppm}^{-1}$ (Norby et al., 2005; Piao et al., 2013). From 2001 to 2015, the CO₂ concentration has increased by 30 ppm (www.esrl.noaa.gov/gmd/ccgg/trends/), and it was calculated that BESS yielded a GPP–CO₂ response of $0.12 \text{ PgC ppm}^{-1}$ ($0.10\% \text{ ppm}^{-1}$ considering the BESS mean annual global GPP of 123 PgC y^{-1}), which was also comparable with the FACE experiment. Whether to include carbon–nitrogen interactions or not is the key factor leading to such large discrepancies (Smith et al., 2015). BESS explicitly utilized CO₂ data as an input of photosynthesis module, and assumed the nitrogen limitation effect might be partially reflected in the canopy structure (McMurtrie et al., 2008; Yin, 2000), which in turn influenced APAR and canopy V_{max}^{25C} . Such process-based approaches ensure that BESS produces a reasonable GPP response to elevated CO₂, which is implemented in neither machine-learning methods nor semi-empirical approaches.

The discrepancies in ET trend were considerable among the three products from 2001 through 2011 (Fig. 5b). During this time period, BESS produced a non-significant descending trend by $-0.07 \times 10^3 \text{ km}^3 \text{ y}^{-2}$ ($p > 0.1$), MPI-BGC produced a non-significant increasing trend by $0.11 \times 10^3 \text{ km}^3 \text{ y}^{-2}$ ($p > 0.1$), while MODIS produced a significant increasing trend by $0.22 \times 10^3 \text{ km}^3 \text{ y}^{-2}$ ($p < 0.05$). Although climate change tends to intensify the water cycle in the long-term (Huntington, 2006), there is a debate of the ET trend in the 21st century. Some reported slightly increasing trend (Yan et al., 2013; Zhang et al., 2015), some found no trend (Badgley et al., 2015; Zeng et al., 2012), and some demonstrated slightly decreasing trends caused by the limited soil moisture supply in South Hemisphere (Jung et al., 2010), a decline in net radiation in tropic and mid-latitude regions (Vinukollu et al., 2011), and the elevated CO₂-induced reduction in stomatal conductance (Mao et al., 2015). As the ET variation is highly influenced by the El Niño–La Niña cycle (Miralles et al., 2013), 15 years data are likely insufficient to conduct a solid ET trend analysis.

Table 8

Comparison of global mean annual GPP and ET estimates derived from BESS, MPI-BGC and MODIS products from 2001 to 2011.

Product	GPP (PgC y^{-1})		ET ($\text{km}^3 \text{ y}^{-1}$)	
	Mean	CI	Mean	CI
BESS	122 \pm 25		$65 \times 10^3 \pm 11 \times 10^3$	
MPI-BGC	120		65×10^3	
MODIS	110 \pm 23		$62 \times 10^3 \pm 13 \times 10^3$	

Table 9

R^2 and RMSE between BESS, MPI-BGC and MODIS global mean annual GPP and ET maps in 0.5° resolution from 2001 to 2011.

Relationship	GPP		ET	
	R^2	RMSE ($\text{gC m}^{-2} \text{ y}^{-1}$)	R^2	RMSE (mm y^{-1})
MPI-BGC–BESS	0.93	229	0.90	118
MODIS–BESS	0.93	244	0.82	160
MPI-BGC–MODIS	0.92	261	0.85	143

Table 10

Mean annual GPP and ET for different plant functional types (PFTs): evergreen needle leaved forest (ENF), evergreen broadleaved forest (EBF), deciduous needle leaved forest (DNF), deciduous broadleaved forest (DBF), mixed forest (MF), open shrublands (OSH), woody savannas (WSA), savannas (SAV), grasslands (GRA), permanent wetlands (WET), and croplands (CRO).

PFT	GPP ($\text{gC m}^{-2} \text{y}^{-1}$)			ET (mm y^{-1})		
	BESS	MPI-BGC	MODIS	BESS	MPI-BGC	MODIS
ENF	677	739	710	285	335	372
EBF	2765	2506	2472	1171	991	1293
DNF	585	584	637	256	299	377
DBF	1101	1429	1329	500	710	608
MF	1037	1118	1045	424	462	533
CSH	579	580	685	603	375	460
OSH	285	295	318	259	252	221
WSA	1750	1569	1498	944	848	830
SAV	1426	1403	1280	898	836	730
GRA	495	407	405	326	338	303
WET	1184	848	1010	626	334	647
CRO	998	973	894	552	583	514
Other	1	4	1	2	4	1

5. Conclusions

A set of global GPP and ET products, derived from remote sensing data and a process-based model, was provided in 8-day interval and 1 km resolution from 2000 to 2015. The products were intensively assessed through direct evaluation against FLUXNET site observations at 8-day, mean monthly and annual scale, as well as an intercomparison of the spatiotemporal patterns and relationships of MPI-BGC and MODIS GPP and ET products globally and decadal. Despite the fundamentally different approaches (process-based versus machine-learning and semi-empirical), BESS GPP and ET products were comparable with existing global products at both site and global levels. In particular, The BESS products were in line with MPI-BGC, which is usually treated as a proxy of upscaled FLUXNET observations, in terms of the overall magnitude, spatial distribution, and interannual variability for both GPP and ET. Furthermore, BESS produced a significant ascending GPP trend (0.27 PgC y^{-2}), consistent with state-of-the-art land surface

Table A1

Look-up table of the maximum leaf carboxylation rate at 25 °C for different plant functional types (PFTs): evergreen needle leaved forest (ENF), evergreen broadleaved forest (EBF), deciduous needle leaved forest (DNF), deciduous broadleaved forest (DBF), mixed forest (MF), shrublands (SHR), savannas (SAV), grasslands (GRA), permanent wetlands (WET), and croplands (CRO).

PFT	Warm	Temperate	Cold
ENF	63 ^a		
EBF	41 ^a	62 ^a	
DNF	57 ^b		
DBF	66 ^c	62 ^c	96 ^c
MF	54 ^d	62 ^e	63 ^f
SHR	62 ^a	54 ^a	
SAV	90 ^g	120 ^h	
GRA (C3)	78 ^a		142 ^c
GRA (C4)		40 ⁱ	
CRO (C3)	101 ^j		
CRO (C4)	37 ^j		
WET	78 ^a		142 ^c

^a (Kattge et al., 2009).

^b (Bonan et al., 2011).

^c (Groenendijk et al., 2011).

^d Average of EBF and DBF.

^e Average of ENF, EBF and DBF.

^f Average of ENF and DBF.

^g (Cernusak et al., 2011; Hutley et al., 2011; Meir et al., 2007; Simioni et al., 2004a).

^h (Xu and Baldocchi, 2003).

ⁱ (Anderson et al., 2001; Domingues et al., 2007; Kubien and Sage, 2004; Simioni et al., 2004b).

^j (Zhang et al., 2014).

models, and much finer spatial and temporal resolution maps than MPI-BGC. We conclude that BESS can serve as a set of independent GPP and ET products from official MODIS correspondences. We expect that the BESS products could advance the progress of global change studies through bridging remote sensing data and land surface models, which was appealed by Sellers et al. (1997) 20 years ago. The products are publically-available at <http://environment.snu.ac.kr/>.

Acknowledgement

This research was funded by National Research Foundation of Korea (NRF-2014R1A2A1A11051134). We thank scientists who had made and shared MPI-BGC and MODIS products, and Microsoft Research which supported initial processing of MODIS data. This work used eddy covariance data acquired and shared by the FLUXNET community, including these networks: AmeriFlux, AfriFlux, AsiaFlux, CarboAfrica, CarboEuropeIP, CarboItaly, CarboMont, ChinaFlux, Fluxnet-Canada, GreenGrass, ICOS, KoFlux, LBA, NECC, OzFlux-TERN, TCOS-Siberia, and USCCC. The FLUXNET eddy covariance data processing and harmonization was carried out by the ICOS Ecosystem Thematic Center, AmeriFlux Management Project and Fluxdata project of FLUXNET, with the support of CDIAC, and the OzFlux, ChinaFlux and AsiaFlux offices.

Appendix A. We improved the model structure and data preprocessing procedure over (Ryu et al., 2011), mainly in terms of the computation effectiveness and efficiency of global long-term (from Marth 1, 2000 to December 31, 2015) high-resolution (1-km) datasets production. Specifically, the major changes included: (1) acceleration of swath data reprojection, (2) modification of data filtering, (3) consideration of the CO₂ fertilization effect, (4) correction of MOD07-derived air temperature, (5) alteration of V_{max}^{25C} parameterization, and (6) refinement of leaf temperature computation.

A.1. Acceleration of swath data reprojection

Previously, reprojection from the MODIS swath spatial reference to the sinusoidal projection system was conducted tile by tile. For each land surface sinusoidal grid tile, all the intersecting swaths were identified by analyzing boundary coordinates. Subsequently, for each tile pixel, the nearest swath pixel was searched by computing the geographic distance. Because one single swath usually involves many grid tiles, especially in high latitude regions, this could cause considerable computation redundancy. In addition, a pixel by pixel distance analysis is rather computation intensive. In this study, for a given day, a global Delaunay triangular network was built directly from all daytime Terra swath data coordinates, and the nearest neighborhood relationships between global sinusoidal pixels and swath data pixels were established by sampling on the global Delaunay triangular network.

A.2. Modification of data filtering

It was shown that the BESS GPP simulation was most sensitive to LAI, followed by the maximum leaf carboxylation rate at 25 °C centigrade V_{max}^{25C} (Ryu et al., 2011). The MOD15A2 8-day composite LAI product was gap-filled using multi-year average main-algorithm values. To further reduce cloud-induced underestimation of LAI, BESS model selected the maximum LAI in an 8-week interval and kept the value over the 8 weeks, but it could only be applied in tropical rainforest where the seasonal variation of the LAI is negligible. To detect and filter cloud-contaminated LAI pixels, regardless of land cover types, two assumptions were made: 1) the cloud contamination leads to an underestimation of LAI, and 2) the actual LAI could not promptly decrease and then promptly increase within a short time period. Considering the case of a single observation x_d at day of year (DOY) d and four observations x_{d-16} , x_{d-8} , x_{d+8} , and x_{d+16} at DOY $d - 16$, $d - 8$, $d + 8$, and

Table A2
Site information.

PFT	Site	Latitude	Longitude	Time	Citation	
Evergreen needleleaf forest (ENF)	AR-Vir	−28.2395	−56.1886	2009–2012	Posse et al. (2016)	
	AU-ASM	−22.283	133.249	2010–2013	Eamus et al. (2013)	
	CA-NS1	55.8792	−98.4839	2002–2005	Goulden et al. (2006)	
	CA-NS3	55.9117	−98.3822	2001–2005	Goulden et al. (2006)	
	CA-NS4	55.9117	−98.3822	2002–2005	Goulden et al. (2006)	
	CA-NS5	55.8631	−98.485	2001–2005	Goulden et al. (2006)	
	CA-Qfo	49.6925	−74.3421	2003–2010	Bergeron et al. (2007)	
	CA-SF1	54.485	−105.818	2003–2006	Mkhabela et al. (2009)	
	CA-SF2	54.2539	−105.878	2001–2005	Mkhabela et al. (2009)	
	CN-Qia	26.7414	115.0581	2003–2005	Yu et al. (2006)	
	CZ-BK1	49.5021	18.5369	2000–2012	Pavelka et al. (2007)	
	DE-Lkb	49.0996	13.3047	2009–2013	Lindauer et al. (2014)	
	DE-Obe	50.7836	13.7196	2008–2014	Zimmermann et al. (2006)	
	DE-Tha	50.9636	13.5669	2000–2014	Grünwald and Bernhofer (2007)	
	FI-Hyy	61.8475	24.295	2000–2014	Vesala et al. (2005)	
	IT-La2	45.9542	11.2853	2000–2002	Cescatti and Zorer (2003)	
	IT-Lav	45.9562	11.2813	2003–2012	Cescatti and Zorer (2003)	
	IT-Ren	46.5869	11.4337	2000–2013	Marcolla et al. (2005)	
	IT-SR2	43.732	10.291	2013–2014	Matteucci et al. (2015)	
	IT-SRo	43.7279	10.2844	2000–2012	Matteucci et al. (2015)	
	NL-Loo	52.1666	5.7436	1996–2013	Dolman et al. (2002)	
	RU-Fyo	56.4615	32.9221	2000–2013	Kurbatova et al. (2008)	
	US-Blo	38.8953	−120.633	2000–2007	Goldstein et al. (2000)	
	US-Me6	44.3233	−121.608	2010–2012	Ruehr et al. (2012)	
	Evergreen broadleaf forest (EBF)	AU-Cum	−33.6133	150.7225	2012–2013	Karan et al. (2016)
		AU-Rob	−17.1175	145.6301	2014–2014	Karan et al. (2016)
AU-Tum		−35.6566	148.1517	2001–2013	Leuning et al. (2005)	
AU-Whr		−36.6732	145.0294	2011–2013	Karan et al. (2016)	
BR-Sa3		−3.018	−54.9714	2000–2004	Miller et al. (2004)	
CN-Din		23.1733	112.5361	2003–2005	Yu et al. (2006)	
FR-Pue		43.7414	3.5958	2000–2013	Rambal et al. (2004)	
GF-Guy		5.2788	−52.9249	2004–2012	Bonal et al. (2008)	
IT-Cp2		41.7043	12.3573	2012–2013	Fares and Loreto (2015)	
Deciduous broadleaf forest (DBF)		DE-Hai	51.0792	10.453	2000–2012	Knohl et al. (2003)
	DK-Sor	55.4859	11.6446	2000–2012	Pilegaard et al. (2001)	
	IT-CA1	42.3804	12.0266	2011–2013	Sabbatini et al. (2016)	
	IT-CA3	42.38	12.0222	2011–2013	Sabbatini et al. (2016)	
	IT-Isp	45.8126	8.6336	2013–2014	Ferréa et al. (2012)	
	IT-PT1	45.2009	9.061	2002–2004	Migliavacca et al. (2009)	
	IT-Ro1	42.4081	11.93	2000–2008	Rey et al. (2002)	
	IT-Ro2	42.3903	11.9209	2002–2012	Tedeschi et al. (2006)	
	JP-MBF	44.3869	142.3186	2003–2005	Yamazaki et al. (2013)	
	US-Ha1	42.5378	−72.1715	2000–2012	Urbanski et al. (2007)	
	US-MMS	39.3232	−86.4131	2000–2014	Schmid et al. (2000)	
	US-UMd	45.5625	−84.6975	2007–2014	Gough et al. (2013)	
	US-WCr	45.8059	−90.0799	2000–2014	Cook et al. (2004)	
	ZM-Mon	−15.4378	23.2528	2007–2009	Scanlon and Albertson (2004)	
	Mixed forest (MF)	AR-SLu	−33.4648	−66.4598	2009–2011	http://www.fluxdata.org:8080/sitepages/siteInfo.aspx?AR-SLu
BE-Bra		51.3092	4.5206	2000–2013	Carrara et al. (2003)	
BE-Vie		50.3051	5.9981	2000–2014	Aubinet et al. (2001)	
CN-Cha		42.4025	128.0958	2003–2005	Zhang et al. (2006)	
JP-SMF		35.2617	137.0788	2002–2006	Yamazaki et al. (2013)	
US-Syv		46.242	−89.3477	2001–2014	Desai et al. (2005)	
Close shrublands (CSH)	IT-Noe	40.6061	8.1515	2004–2012	Spano et al. (2005)	
Open shrublands (OSH)	CA-NS6	55.9167	−98.9644	2001–2005	Goulden et al. (2006)	
	CA-NS7	56.6358	−99.9483	2002–2005	Goulden et al. (2006)	
	CA-SF3	54.0916	−106.005	2001–2006	Mkhabela et al. (2009)	
	ES-LgS	37.0979	−2.9658	2007–2009	Reverter et al. (2010)	
	ES-Ln2	36.9695	−3.4758	2009–2009	Marañón-Jiménez et al. (2011)	
	RU-Cok	70.8291	147.4943	2003–2013	Dolman et al. (2012)	
	US-Whs	31.7438	−110.052	2007–2014	Scott (2010)	
Woody savannas (WSA)	AU-Ade	−13.0769	131.1178	2007–2009	Beringer et al. (2011)	
	AU-RDF	−14.5636	132.4776	2011–2013	Beringer et al. (2011)	
	US-SRM	31.8214	−110.866	2004–2014	Scott (2010)	
	US-Ton	38.4316	−120.966	2001–2014	Baldocchi et al. (2004)	
Savannas (SAV)	AU-Cpr	−34.0021	140.5891	2010–2013	Karan et al. (2016)	
	AU-DaS	−14.1593	131.3881	2008–2013	Beringer et al. (2011)	
	AU-Dry	−15.2588	132.3706	2008–2013	Beringer et al. (2011)	
	AU-GWW	−30.1913	120.6541	2013–2014	Prober et al. (2012)	
	SD-Dem	13.2829	30.4783	2005–2009	Sjöström et al. (2008)	
	ZA-Kru	−25.0197	31.4969	2000–2010	Scholes et al. (2001)	
Grasslands (GRA)	AT-Neu	47.1167	11.3175	2002–2012	Wohlfahrt et al. (2008)	
	AU-DaP	−14.0633	131.3181	2008–2013	Beringer et al. (2011)	

(continued on next page)

Table A2 (continued)

PFT	Site	Latitude	Longitude	Time	Citation
	AU-Emr	−23.8587	148.4746	2011–2013	Schroder (2014)
	AU-Rig	−36.6499	145.5759	2011–2013	Beringer et al. (2011)
	CH-Cha	47.2102	8.4104	2006–2012	Eugster and Zeeman (2006)
	CH-Fru	47.1158	8.5378	2006–2012	Eugster and Zeeman (2006)
	CH-Oe1	47.2858	7.7319	2002–2008	Ammann et al. (2007)
	CN-Cng	44.5934	123.5092	2007–2010	Dong et al. (2011)
	CN-Dan	30.4978	91.0664	2004–2005	Yu et al. (2006)
	CN-Du2	42.0467	116.2836	2006–2008	Chen et al. (2009)
	CN-HaM	37.37	101.18	2002–2004	Kato et al. (2006)
	CN-Sw2	41.7902	111.8971	2010–2012	Shao et al. (2013b)
	CZ-BK2	49.4944	18.5429	2004–2011	Pavelka et al. (2007)
	DE-Gri	50.9495	13.5125	2004–2014	Gilmanov et al. (2007)
	DK-ZaH	74.4732	−20.5503	2000–2009	Lund et al. (2012)
	IT-Tor	45.8444	7.5781	2008–2013	Galvagno et al. (2013)
	NL-Hor	52.2404	5.0713	2004–2011	van der Molen et al. (2004)
	RU-Ha1	54.7252	90.0022	2002–2004	Marchesini et al. (2007)
	US-AR1	36.4267	−99.42	2009–2012	Billesbach and Bradford (2016)
	US-AR2	36.6358	−99.5975	2009–2012	Billesbach and Bradford (2016)
	US-Var	38.4133	−120.951	2000–2014	Ma et al. (2007)
	US-Wkg	31.7365	−109.942	2004–2014	Scott (2016)
Permenent wetlands (WET)	AU-Fog	−12.5452	131.3072	2006–2008	Beringer et al. (2011))
	CN-Ha2	37.6086	101.3269	2003–2005	Fu et al. (2006)
	DE-Akm	53.8662	13.6834	2009–2014	http://www.fluxdata.org:8080/sitepages/siteInfo.aspx?DE-Akm
	DE-Spw	51.8923	14.0337	2010–2014	http://www.fluxdata.org:8080/sitepages/siteInfo.aspx?DE-spw
	DK-NuF	64.1308	−51.3861	2008–2014	Westergaard-Nielsen et al. (2013)
	NO-Adv	78.186	15.923	2011–2014	Pirk et al. (2016)
	RU-Che	68.613	161.3414	2002–2005	Merboid et al. (2009)
	US-Los	46.0827	−89.9792	2000–2014	Sulman et al. (2009)
	US-Myb	38.0498	−121.765	2011–2014	Sturtevant et al. (2016)
	Croplands (CRO)	BE-Lon	50.5516	4.7461	2004–2014
DE-Kli		50.8929	13.5225	2004–2014	Ceschia et al. (2010)
DE-RuS		50.8659	6.4472	2011–2014	Mauder et al. (2013)
FI-Jok		60.8986	23.5135	2000–2003	Gilmanov et al. (2007)
FR-Gri		48.8442	1.9519	2004–2013	Loubet et al. (2011)
IT-CA2		42.3772	12.026	2011–2013	Sabbatini et al. (2016)
US-ARM		36.6058	−97.4888	2003–2012	Fischer et al. (2007)
US-Ne1		41.1651	−96.4766	2001–2013	Verma et al. (2005)
US-Ne2		41.1649	−96.4701	2001–2013	Verma et al. (2005)
US-Ne3		41.1797	−96.4397	2001–2013	Verma et al. (2005)
US-Tw3	38.1159	−121.647	2013–2014	Baldocchi (2016)	

$d + 16$, respectively, where 8 is the MODIS LAI data cycle, x_d is judged as contaminated LAI data if it meets the conditions: 1) $[\max(x_{d-16}, x_{d-8}) - x_d] / \max(x_{d-16}, x_{d-8}) > t$ and 2) $[\max(x_{d+8}, x_{d+16}) - x_d] / \max(x_{d+8}, x_{d+16}) > t$, where the change rate threshold t was set as 0.5 or 20% which are the targeted absolute and relative uncertainty of satellite LAI products (<http://www.wmo.int/pages/prog/gcos/Publications/gcos-154.pdf>). The cloud-contaminated LAI values were replaced by the mean value of $\max(x_{d-16}, x_{d-8})$ and $\max(x_{d+8}, x_{d+16})$. The filter procedure was applied to the gap-filled LAI data and was first run from DOY 1 towards DOY 365 and then backwards.

The V_{max}^{25C} in BESS was determined by two biome-based look-up tables. In the previous version, the MCD12Q1 yearly land cover type product was used directly. We found that in some cases, the land cover type fluctuates over the years, causing unexpected interannual variations in V_{max}^{25C} , which are subsequently propagated to GPP products. To avoid such unrealistic annual GPP fluctuations, the MODIS land cover products were composited into one according to the maximum frequency over all the available years (2001–2013) for each pixel. Additionally, one IGBP land cover type, cropland/Natural vegetation mosaic, was difficult to parameterize for V_{max}^{25C} , and was replaced by the secondary land cover type defined in the MCD12Q1 dataset.

A.3. Consideration of the CO₂ fertilization effect

In the previous BESS, both ambient and intercellular CO₂ concentrations (C_a and C_i) were fixed. C_a was set as 380 ppm and the ratios of C_i to C_a were set as 0.7 and 0.4 for C3 and C4 plants, respectively. To consider

the CO₂ fertilization effect, we first generated monthly composite 5-km resolution C_a maps in 2015 by interpolating Orbiting Carbon Observatory-2 (OCO-2) Lite Version-7 XCO₂ dataset. To account for the temporal evolution of C_a from 2001 to 2014, we subtracted the annual C_a changing rate (www.esrl.noaa.gov/gmd/ccgg/trends/) from the 2015 monthly maps, assuming these rates were globally and yearly representative. Furthermore, we considered the spatiotemporal variations of C_i by incorporating it in the iteration procedure (Fig. 1). At each iteration, the sunlit/shade canopy C_i of C3 and C4 plants was calculated after the computation of photosynthesis by:

$$g_b = \frac{1}{r_a} \quad (A1)$$

$$C_s = C_a - \frac{A_n}{g_b} \quad (A2)$$

$$g_s = m \times \frac{RH \times A_n}{C_s} + b_0 \quad (A3)$$

$$C_i = C_s - 1.6 \times \frac{A_n}{g_s} \quad (A4)$$

where r_a , g_b , C_s , A_n , g_s , RH , m , b_0 are the aerodynamic resistance, boundary layer H₂O conductance, leaf surface CO₂ concentration, net CO₂ assimilation, stomatal H₂O conductance, relative humidity, Ball-Berry function slope and intercept, respectively.

A.4. Correction of MOD07-derived air temperature

Clear-sky air temperature and dew point temperature were derived from reprojected MODIS atmosphere profile product by the hypsometric equation (Wallace and Hobbs, 1977). Nevertheless, we found large biases existed in MOD07-derived air temperature and dew point temperature in some cases. To address this issue, we used the ERA Interim Reanalysis to make a correction. The ERA 2 m air temperature and dew point temperature data were provided in $0.75 \times 0.75^\circ$ resolution at 3-h intervals. We first applied a bi-linear spatial interpolation to ERA data to match the MODIS spatial resolution (5 km). Then, for each pixel we applied a linear temporal interpolation to match the Terra overpass time. For each climate zone the mean values of ERA-derived temperatures and MOD07-derived temperatures were computed, and the ratios were used to correct the MOD07-derived temperatures.

A.5. Alteration of V_{max}^{25C} parameterization

An albedo-nitrogen relation for closed-canopy temperate and boreal forests was used in the previous study. However, a recent study showed that such relation might not be direct at the satellite-level, without accounting for canopy structural effects (Knyazikhin et al., 2013). Therefore, the relationship was not used in this study. All peak V_{max}^{25C} values were parameterized using an updated look-up-table based on PFTs and climatic zones (Table A1).

A.6. Refinement of leaf temperature computation.

Theoretically, leaf temperature is driven by the available energy, but it also influences the latter through emitting longwave radiation. For simplicity, however, the old version BESS did not explicitly consider the leaf longwave radiation balance when it calculated leaf temperature. In the improved version, we used a longwave radiation transfer developed in the Commonwealth Scientific and Industrial Research Organisation (CSIRO) Atmosphere Biosphere Land Exchange (CABLE) model (Wang et al., 2006):

$$Q_{LW, Sun} = \frac{(\varepsilon_s \sigma T_s^4 - \varepsilon_f \sigma T_f^4) k_d (e^{-k_d LAI} - e^{-k_b LAI})}{k_d - k_b} + \frac{k_d (\varepsilon_a \sigma T_a^4 - \varepsilon_f \sigma T_f^4) [1 - e^{-(k_b + k_d) LAI}]}{k_d + k_b} \quad (A5)$$

$$Q_{LW, Sh} = [1 - e^{-k_d LAI}] (\varepsilon_s \sigma T_s^4 + \varepsilon_a \sigma T_a^4 - 2\varepsilon_f \sigma T_f^4) - Q_{LW, Sun} \quad (A6)$$

$$Q_{LW, Soil} = \varepsilon_f \sigma T_f^4 (1 - e^{-k_d LAI}) + \varepsilon_a \sigma T_a^4 e^{-k_d LAI} \quad (A7)$$

where k_b and k_d refer to extinction coefficients for beam and scattered longwave radiation for black leaves, respectively, σ is the Stefan Boltzmann constant, ε_f , ε_s , and ε_a are the emissivity for leaf, soil and air, respectively, and T_f , T_s , and T_a are the corresponding temperatures. The leaf temperature T_f is the weighted sum of the sunlit/shade components according to the fraction of sunfleck penetration f_{Sun}

$$T_f = T_{f, Sun} f_{Sun} + T_{f, Sh} (1 - f_{Sun}) \quad (A8)$$

Subsequently, the canopy net radiation for sunlit/shade components and soil net radiation can be calculated by

$$R_{n,i} = Q_{PAR,i} + Q_{NIR,i} + Q_{LW,i} - 4\varepsilon_s \sigma T_a^3 (T_{f,i} - T_a) \quad (A9)$$

$$R_{Soil} = Q_{PAR,Soil} + Q_{NIR,Soil} + Q_{LW,Soil} - 4\varepsilon_s \sigma T_a^3 (T_s - T_a) \quad (A10)$$

where $i = Sun$ or Sh indicate sunlit or shade leaf, respectively. After computing the sunlit/shade canopy latent heat of ($\lambda E_{n,i}$) by solving

the quadratic form of the Penman–Monteith equation, and soil latent heat (λE_{Soil}) and heat storage (G_{Soil}) by using an empirical function (Ryu et al., 2011), the leaf temperature and soil temperature were updated by

$$T_{f,i} - T_a = \frac{r_a (R_{n,i} - \lambda E_{n,i})}{\rho_a C_p} \quad (A11)$$

$$T_s - T_a = \frac{r_a (R_{Soil} - \lambda E_{Soil} - G_{Soil})}{\rho_a C_p} \quad (A12)$$

At this point, the derived component temperatures were updated in the iteration procedure (Fig. 1).

References

- Ammann, C., Flechard, C.R., Leifeld, J., Neftel, A., Fuhrer, J., 2007. The carbon budget of newly established temperate grassland depends on management intensity. *Agric. Ecosyst. Environ.* 121 (1), 5–20. <http://dx.doi.org/10.1016/j.agee.2006.12.002>.
- Anav, A., Friedlingstein, P., Beer, C., Ciais, P., Harper, A., et al., 2015. Spatio-temporal patterns of terrestrial gross primary production: a review. *Rev. Geophys.* 53 (3), 785–818. <http://dx.doi.org/10.1002/2015RG000483>.
- Anav, A., Murray-Tortarolo, G., Friedlingstein, P., Sitch, S., Piao, S., et al., 2013. Evaluation of land surface models in reproducing satellite derived leaf area index over the high-latitude northern hemisphere. Part II: Earth system models. *Remote Sens.* 5 (8), 3637–3661. <http://dx.doi.org/10.3390/rs5083637>.
- Anderson, L.J., Maherali, H., Johnson, H.B., Polley, H.W., Jackson, R.B., 2001. Gas exchange and photosynthetic acclimation over subambient to elevated CO₂ in a C3-C4 grassland. *Glob. Chang. Biol.* 7 (6), 693–707. <http://dx.doi.org/10.1046/j.1354-1013.2001.00438.x>.
- Aubinet, M., Chermanne, B., Vandenhaute, M., Longdoz, B., Yernaux, M., et al., 2001. Long term carbon dioxide exchange above a mixed forest in the Belgian Ardennes. *Agric. For. Meteorol.* 108 (4), 293–315. [http://dx.doi.org/10.1016/S0168-1923\(01\)00244-1](http://dx.doi.org/10.1016/S0168-1923(01)00244-1).
- Badgley, G., Fisher, J.B., Jiménez, C., Tu, K.P., Vinukollu, R., 2015. On uncertainty in global terrestrial evapotranspiration estimates from choice of input forcing datasets. *J. Hydrometeorol.* 16 (4), 1449–1455. <http://dx.doi.org/10.1175/JHM-D-14-0040.1>.
- Baldocchi, D., 2016. AmeriFlux US-Tw3 Twitchell Alfalfa. AmeriFlux. <http://dx.doi.org/10.17190/AMF/1246149>.
- Baldocchi, D.D., Xu, L., Kiang, N., 2004. How plant functional-type, weather, seasonal drought, and soil physical properties alter water and energy fluxes of an oak-grass savanna and an annual grassland. *Agric. For. Meteorol.* 123 (1), 13–39. <http://dx.doi.org/10.1016/j.agrformet.2003.11.006>.
- Ball, J.T., 1988. *An Analysis of Stomata Conductance*. Stanford University.
- Beer, C., Reichstein, M., Tomelleri, E., Ciais, P., Jung, M., et al., 2010. Terrestrial gross carbon dioxide uptake: global distribution and covariation with climate. *Science* 329 (August), 834–838.
- Bergeron, O., Margolis, H.A., Black, T.A., Coursolle, C., Dunn, A.L., et al., 2007. Comparison of carbon dioxide fluxes over three boreal black spruce forests in Canada. *Glob. Chang. Biol.* 13 (1), 89–107. <http://dx.doi.org/10.1111/j.1365-2486.2006.01281.x>.
- Beringer, J., Hutley, L.B., Hacker, J.M., Neininger, B., Paw U, K.T., 2011. Patterns and processes of carbon, water and energy cycles across northern Australian landscapes: from point to region. *Agric. For. Meteorol.* 151 (11), 1409–1416. <http://dx.doi.org/10.1016/j.agrformet.2011.05.003>.
- Billesbach, D., Bradford, J., 2016. AmeriFlux US-AR1 ARM USDA UNL OSU Woodward Switchgrass 1. AmeriFlux. <http://dx.doi.org/10.17190/AMF/1246137>.
- Bonal, D., Bosc, A., Ponton, S., Goret, J.Y., Burban, B.T., et al., 2008. Impact of severe dry season on net ecosystem exchange in the Neotropical rainforest of French Guiana. *Glob. Chang. Biol.* 14 (8), 1917–1933. <http://dx.doi.org/10.1111/j.1365-2486.2008.01610.x>.
- Bonan, G.B., Lawrence, P.J., Oleson, K.W., Levis, S., Jung, M., et al., 2011. Improving canopy processes in the Community Land Model version 4 (CLM4) using global flux fields empirically inferred from FLUXNET data. *J. Geophys. Res.* 116 (G2), G02014. <http://dx.doi.org/10.1029/2010JG001593>.
- Carrara, A., Kowalski, A.S., Neiryneck, J., Janssens, I.A., Yuste, J.C., et al., 2003. Net ecosystem CO₂ exchange of mixed forest in Belgium over 5 years. *Agric. For. Meteorol.* 119 (3), 209–227. [http://dx.doi.org/10.1016/S0168-1923\(03\)00120-5](http://dx.doi.org/10.1016/S0168-1923(03)00120-5).
- Cernuska, L.A., Hutley, L.B., Beringer, J., Holtum, J.A.M., Turner, B.L., 2011. Photosynthetic physiology of eucalypts along a sub-continent rainfall gradient in northern Australia. *Agric. For. Meteorol.* 151 (11), 1462–1470. <http://dx.doi.org/10.1016/j.agrformet.2011.01.006>.
- Cescatti, A., Zorer, R., 2003. Structural acclimation and radiation regime of silver fir (*Abies alba* Mill.) shoots along a light gradient. *Plant Cell Environ.* 26 (3), 429–442. <http://dx.doi.org/10.1046/j.1365-3040.2003.00974.x>.
- Ceschia, E., Béziat, P., Dejoux, J.F., Aubinet, M., Bernhofer, C., et al., 2010. Management effects on net ecosystem carbon and GHG budgets at European crop sites. *Agric. Ecosyst. Environ.* 139 (3), 363–383. <http://dx.doi.org/10.1016/j.agee.2010.09.020>.
- Chen, S., Chen, J., Lin, G., Zhang, W., Miao, H., et al., 2009. Energy balance and partition in Inner Mongolia steppe ecosystems with different land use types. *Agric. For. Meteorol.* 149 (11), 1800–1809. <http://dx.doi.org/10.1016/j.agrformet.2009.06.009>.
- Chen, B., Liu, J., Chen, J., Croft, H., Gonsamo, A., et al., 2016. Assessment of foliage clumping effects on evapotranspiration estimates in forested ecosystems. *Agric. For. Meteorol.* 216, 82–92. <http://dx.doi.org/10.1016/j.agrformet.2015.09.017>.

- Chen, J., Mo, G., Pisek, J., Liu, J., Deng, F., et al., 2012. Effects of foliage clumping on the estimation of global terrestrial gross primary productivity. *Glob. Biogeochem. Cycles* 26 (1), 1–18. <http://dx.doi.org/10.1029/2010GB003996>.
- Collatz, G.J., Ribas-Carbo, M., Berry, J.A., 1992. Coupled photosynthesis-stomatal conductance model for leaves of C4 plants. *Aust. J. Plant Physiol.* 19 (5), 519–539. <http://dx.doi.org/10.1071/PP9920519>.
- Cook, B.D., Davis, K.J., Wang, W., Desai, A., Berger, B.W., et al., 2004. Carbon exchange and venting anomalies in an upland deciduous forest in northern Wisconsin, USA. *Agric. For. Meteorol.* 126 (3), 271–295. <http://dx.doi.org/10.1016/j.agrformet.2004.06.008>.
- Dai, Y., Zeng, X., Dickinson, R.E., Baker, I., Bonan, G.B., et al., 2003. The Common Land Model. *Bull. Am. Meteorol. Soc.* 84 (8), 1013–1023. <http://dx.doi.org/10.1175/BAMS-84-8-1013>.
- De Pury, D.G.G., Farquhar, G.D., 1997. Simple scaling of photosynthesis from leaves to canopies without the errors of big-leaf models. *Plant Cell Environ.* 20 (5), 537–557. <http://dx.doi.org/10.1111/j.1365-3040.1997.tb00466.x>.
- Desai, A.R., Bolstad, P.V., Cook, B.D., Davis, K.J., Carey, E.V., 2005. Comparing net ecosystem exchange of carbon dioxide between an old-growth and mature forest in the upper Midwest, USA. *Agric. For. Meteorol.* 128 (1), 33–55. <http://dx.doi.org/10.1016/j.agrformet.2004.09.005>.
- Dickinson, R.E., 1983. Land surface processes and climate-surface albedos and energy balance. *Adv. Geophys.* 25, 305–353.
- Dirmeyer, P.A., Gao, X., Zhao, M., Guo, Z., Oki, T., et al., 2006. GSWP-2: multimodel analysis and implications for our perception of the land surface. *Bull. Am. Meteorol. Soc.* 87 (10), 1381–1397. <http://dx.doi.org/10.1175/BAMS-87-10-1381>.
- D'Odorico, P., Gonsamo, A., Pinty, B., Gobron, N., Coops, N., et al., 2014. Intercomparison of fraction of absorbed photosynthetically active radiation products derived from satellite data over Europe. *Remote Sens. Environ.* 142, 141–154. <http://dx.doi.org/10.1016/j.rse.2013.12.005>.
- Dolman, A.J., Moors, E.J., Elbers, J.A., 2002. The carbon uptake of a mid latitude pine forest growing on sandy soil. *Agric. For. Meteorol.* 111 (3), 157–170. [http://dx.doi.org/10.1016/S0168-1923\(02\)00024-2](http://dx.doi.org/10.1016/S0168-1923(02)00024-2).
- Dolman, A.J., Shvidenko, A., Schepaschenko, D., Ciais, P., Tchekakova, N., et al., 2012. An estimate of the terrestrial carbon budget of Russia using inventory-based, eddy covariance and inversion methods. *Biogeosciences* 9 (12), 5323–5340. <http://dx.doi.org/10.5194/bg-9-5323-2012>.
- Domingues, T.F., Martinelli, L.A., Ehleringer, J.R., 2007. Ecophysiological traits of plant functional groups in forest and pasture ecosystems from eastern Amazonia, Brazil. *Plant Ecol.* 193 (1), 101–112. <http://dx.doi.org/10.1007/s11258-006-9251-z>.
- Dong, G., Guo, J., Chen, J., Sun, G., Gao, S., et al., 2011. Effects of spring drought on carbon sequestration, evapotranspiration and water use efficiency in the songnen meadow steppe in northeast China. *Ecology* 4 (2), 211–224. <http://dx.doi.org/10.1002/eco.200>.
- Donohue, R.J., Hume, I.H., Roderick, M.L., McVicar, T.R., Beringer, J., et al., 2014. Evaluation of the remote-sensing-based DIFFUSE model for estimating photosynthesis of vegetation. *Remote Sens. Environ.* 155, 349–365. <http://dx.doi.org/10.1016/j.rse.2014.09.007>.
- Dorigo, W., de Jeu, R., Chung, D., Parinussa, R., Liu, Y., et al., 2012. Evaluating global trends (1988–2010) in harmonized multi-satellite surface soil moisture. *Geophysical Research Letters* 39 (18), n/a. <http://dx.doi.org/10.1029/2012GL052988>.
- Eamus, D., Cleverly, J., Boulain, N., Grant, N., Faux, R., et al., 2013. Carbon and water fluxes in an arid-zone acacia savanna woodland: an analyses of seasonal patterns and responses to rainfall events. *Agric. For. Meteorol.* 182–183, 225–238. <http://dx.doi.org/10.1016/j.agrformet.2013.04.020>.
- Eugster, W., Zeeman, M.J., 2006. Micrometeorological techniques to measure ecosystem-scale greenhouse gas fluxes for model validation and improvement. *Int. Congr. Ser.* 1293, 66–75. <http://dx.doi.org/10.1016/j.ijcs.2006.05.001>.
- Fang, H., Liang, S., Hoogenboom, G., 2011. Integration of MODIS LAI and vegetation index products with the CSM-CERES-Maize model for corn yield estimation. *Int. J. Remote Sens.* 32 (4), 1039–1065. <http://dx.doi.org/10.1080/01431160903505310>.
- Fares, S., Loreto, F., 2015. Isoprenoid emissions by the Mediterranean vegetation in Castelporziano. *Rendiconti Lincei* 26 (S3), 493–498. <http://dx.doi.org/10.1007/s12210-014-0331-z>.
- Farquhar, G.D., Caemmerer, S.V., Berry, J.A., 1980. A biochemical model of photosynthetic CO₂ assimilation in leaves of C3 species. *Planta* 90, 78–90. <http://dx.doi.org/10.1007/BF00386231>.
- Ferrá, C., Zenone, T., Comolli, R., Seufert, G., 2012. Estimating heterotrophic and autotrophic soil respiration in a semi-natural forest of Lombardy, Italy. *Pedobiologia* 55 (6), 285–294. <http://dx.doi.org/10.1016/j.pedobi.2012.05.001>.
- Fischer, M.L., Billesbach, D.P., Berry, J.A., Riley, W.J., Torn, M.S., 2007. Spatiotemporal variations in growing season exchange of CO₂, H₂O, and sensible heat in agricultural fields of the southern Great Plains. *Earth Interact.* 11 (1).
- Fisher, J.B., Tu, K.P., Baldocchi, D.D., 2008. Global estimates of the land-atmosphere water flux based on monthly AVHRR and ISLSCP-II data, validated at 16 FLUXNET sites. *Remote Sens. Environ.* 112, 901–919. <http://dx.doi.org/10.1016/j.rse.2007.06.025>.
- Frankenberg, C., Fisher, J.B., Worden, J., Badgley, G., Saatchi, S.S., et al., 2011. New global observations of the terrestrial carbon cycle from GOSAT: patterns of plant fluorescence with gross primary productivity. *Geophys. Res. Lett.* 38 (17), 1–6. <http://dx.doi.org/10.1029/2011GL048738>.
- Friedl, M.A., Sulla-Menashe, D., Tan, B., Schneider, A., Ramankutty, N., et al., 2010. MODIS Collection 5 global land cover: algorithm refinements and characterization of new datasets. *Remote Sens. Environ.* 114 (1), 168–182. <http://dx.doi.org/10.1016/j.rse.2009.08.016>.
- Fu, Y.-L., Yu, G.-R., Sun, X.-M., Li, Y.-N., Wen, X.-F., et al., 2006. Depression of net ecosystem CO₂ exchange in semi-arid *Leymus chinensis* steppe and alpine shrub. *Agric. For. Meteorol.* 137 (3), 234–244. <http://dx.doi.org/10.1016/j.agrformet.2006.02.009>.
- Galvagno, M., Wohlfahrt, G., Cremonese, E., Rossini, M., Colombo, R., et al., 2013. Phenology and carbon dioxide source/sink strength of a subalpine grassland in response to an exceptionally short snow season. *Environ. Res. Lett.* 8 (2), 025008. <http://dx.doi.org/10.1088/1748-9326/8/2/025008>.
- Garrigues, S., Lacaze, R., Baret, F., Morisette, J.T., Weiss, M., et al., 2008. Validation and inter-comparison of global Leaf Area Index products derived from remote sensing data. *J. Geophys. Res. Biogeosci.* 113. <http://dx.doi.org/10.1029/2007JG000635>.
- Gilmanov, T.G., Soussana, J.F., Aires, L., Allard, V., Ammann, C., et al., 2007. Partitioning European grassland net ecosystem CO₂ exchange into gross primary productivity and ecosystem respiration using light response function analysis. *Agric. Ecosyst. Environ.* 121 (1), 93–120. <http://dx.doi.org/10.1016/j.agee.2006.12.008>.
- Goldstein, A.H., Hultman, N.E., Fracheboud, J.M., Bauer, M.R., Panek, J.A., et al., 2000. Effects of climate variability on the carbon dioxide, water, and sensible heat fluxes above a ponderosa pine plantation in the Sierra Nevada (CA). *Agric. For. Meteorol.* 101 (2–3), 113–129. [http://dx.doi.org/10.1016/S0168-1923\(99\)00168-9](http://dx.doi.org/10.1016/S0168-1923(99)00168-9).
- Gough, C.M., Hardiman, B.S., Nave, L.E., Bohrer, G., Maurer, K.D., et al., 2013. Sustained carbon uptake and storage following moderate disturbance in a Great Lakes forest. *Ecol. Appl.* 23 (5), 1202–1215. <http://dx.doi.org/10.1890/1524-1554.1>.
- Goulden, M.L., Winston, G.C., Mcmillan, A.M.S., Litvak, M.E., Read, E.L., et al., 2006. An eddy covariance mesonet to measure the effect of forest age on land-atmosphere exchange. *Glob. Chang. Biol.* 12 (11), 2146–2162. <http://dx.doi.org/10.1111/j.1365-2486.2006.01251.x>.
- Groenendijk, M., Dolman, A.J., Ammann, C., Arneth, A., Pescatti, A., et al., 2011. Seasonal variation of photosynthetic model parameters and leaf area index from global Fluxnet eddy covariance data. *J. Geophys. Res.* 116 (G4), G04027. <http://dx.doi.org/10.1029/2011JG001742>.
- Grünwald, T., Bernhofer, C., 2007. A decade of carbon, water and energy flux measurements of an old spruce forest at the Anchor Station Tharandt. *Tellus, Series B: Chemical and Physical Meteorology* 59. Blackwell Publishing Ltd., pp. 387–396. <http://dx.doi.org/10.1111/j.1600-0889.2007.00259.x>.
- Hazarika, M.K., Yasuoka, Y., Ito, A., Dye, D., et al., 2005. Estimation of net primary productivity by integrating remote sensing data with an ecosystem model. *Remote Sens. Environ.* 94 (3), 298–310. <http://dx.doi.org/10.1016/j.rse.2004.10.004>.
- He, L., Chen, J.M., Pisek, J., Schaaf, C.B., Strahler, A.H., 2012. Global clumping index map derived from the MODIS BRDF product. *Remote Sens. Environ.* 119, 118–130. <http://dx.doi.org/10.1016/j.rse.2011.12.008>.
- Huang, M., Piao, S., Sun, Y., Ciais, P., Cheng, L., et al., 2015. Change in terrestrial ecosystem water-use efficiency over the last three decades. *Glob. Chang. Biol.* 21 (6), 2366–2378. <http://dx.doi.org/10.1111/gcb.12873>.
- Huntington, T.G., 2006. Evidence for intensification of the global water cycle: review and synthesis. *J. Hydrol.* 319 (1–4), 83–95. <http://dx.doi.org/10.1016/j.jhydrol.2005.07.003>.
- Hutley, L.B., Beringer, J., Isaac, P.R., Hacker, J.M., Cernusak, L.A., 2011. A sub-continental scale living laboratory: spatial patterns of savanna vegetation over a rainfall gradient in northern Australia. *Agric. For. Meteorol.* 151 (11), 1417–1428. <http://dx.doi.org/10.1016/j.agrformet.2011.03.002>.
- Ichii, K., Kondo, M., Lee, Y.H., Wang, S.Q., Kim, J., et al., 2013. Site-level model-data synthesis of terrestrial carbon fluxes in the CarboEastAsia eddy-covariance observation network: Toward future modeling efforts. *J. For. Res.* 18 (1), 13–20. <http://dx.doi.org/10.1007/s10310-012-0367-9>.
- Jarvis, A., Reuter, H.I., Nelson, A., Guevara, E., 2008. Hole-filled SRTM for the Globe Version 4. Retrieved from <http://srtm.csi.cgiar.org>.
- Jung, M., Reichstein, M., Bondeau, A., 2009. Towards global empirical upscaling of FLUXNET eddy covariance observations: validation of a model tree ensemble approach using a biosphere model. *Biogeosci. Discuss.* 6 (3), 5271–5304. <http://dx.doi.org/10.5194/bgd-6-5271-2009>.
- Jung, M., Reichstein, M., Ciais, P., Seneviratne, S.I., Sheffield, J., et al., 2010. Recent decline in the global land evapotranspiration trend due to limited moisture supply. *Nature* 467 (7318), 951–954. <http://dx.doi.org/10.1038/nature09396>.
- Jung, M., Reichstein, M., Margolis, H.A., Pescatti, A., Richardson, A.D., et al., 2011. Global patterns of land-atmosphere fluxes of carbon dioxide, latent heat, and sensible heat derived from eddy covariance, satellite, and meteorological observations. *Journal of Geophysical Research* 116, G00J07. <http://dx.doi.org/10.1029/2010JG001566>.
- Karan, M., Liddell, M., Arndt, S., Beringer, J., Boer, M., et al., 2016. The Australian SuperSite Network: a new approach to establishing a continental, long-term terrestrial ecosystem observatory. *Sci. Total Environ.* <http://dx.doi.org/10.1016/j.scitotenv.2016.05.170> (Submitted).
- Kato, T., Tang, Y., Gu, S., Hirota, M., Du, M., et al., 2006. Temperature and biomass influences on interannual changes in CO₂ exchange in an alpine meadow on the Qinghai-Tibetan Plateau. *Glob. Chang. Biol.* 12 (7), 1285–1298. <http://dx.doi.org/10.1111/j.1365-2486.2006.01153.x>.
- Kattge, J., Díaz, S., Lavorel, S., Prentice, I.C., Leadley, P., et al., 2011. TRY - a global database of plant traits. *Glob. Chang. Biol.* 17 (9), 2905–2935. <http://dx.doi.org/10.1111/j.1365-2486.2011.02451.x>.
- Kattge, J., Knorr, W., Raddatz, T., Wirth, C., 2009. Quantifying photosynthetic capacity and its relationship to leaf nitrogen content for global-scale terrestrial biosphere models. *Glob. Chang. Biol.* 15 (4), 976–991. <http://dx.doi.org/10.1111/j.1365-2486.2008.01744.x>.
- Keenan, T.F., Baker, I., Barr, A., Ciais, P., Davis, K., et al., 2012. Terrestrial biosphere model performance for inter-annual variability of land-atmosphere CO₂ exchange. *Glob. Chang. Biol.* 18 (6), 1971–1987. <http://dx.doi.org/10.1111/j.1365-2486.2012.02678.x>.
- Knobl, A., Schulze, E.D., Kolle, O., Buchmann, N., 2003. Large carbon uptake by an unmanaged 250-year-old deciduous forest in Central Germany. *Agric. For. Meteorol.* 118 (3–4), 151–167. [http://dx.doi.org/10.1016/S0168-1923\(03\)00115-1](http://dx.doi.org/10.1016/S0168-1923(03)00115-1).
- Knyazikhin, Y., Lewis, P., Disney, M.L., Stenberg, P., Mottus, M., et al., 2013. Reply to Townsend et al.: decoupling contributions from canopy structure and leaf optics is

- critical for remote sensing leaf biochemistry. *Proc. Natl. Acad. Sci.* 110 (12), E1075. <http://dx.doi.org/10.1073/pnas.1301247110>.
- Kobayashi, H., Iwabuchi, H., 2008. A coupled 1-D atmosphere and 3-D canopy radiative transfer model for canopy reflectance, light environment, and photosynthesis simulation in a heterogeneous landscape. *Remote Sens. Environ.* 112 (1), 173–185. <http://dx.doi.org/10.1016/j.rse.2007.04.010>.
- Kubien, D.S., Sage, R.F., 2004. Low-temperature photosynthetic performance of a C4 grass and a co-occurring C3 grass native to high latitudes. *Plant Cell Environ.* 27 (7), 907–916. <http://dx.doi.org/10.1111/j.1365-3040.2004.01196.x>.
- Kurbatova, J., Li, C., Varlagin, A., Xiao, X., Vygodskaya, N., 2008. Modeling carbon dynamics in two adjacent spruce forests with different soil conditions in Russia. *Biogeosciences* 5, 969–980. <http://dx.doi.org/10.5194/bg-5-969-2008>.
- Lawrence, P.J., Chase, T.N., 2007. Representing a new MODIS consistent land surface in the Community Land Model (CLM 3.0). *J. Geophys. Res. Biogeosci.* 112 (1). <http://dx.doi.org/10.1029/2006JG000168>.
- Leuning, R., Cleugh, H.A., Zegelin, S.J., Hughes, D., 2005. Carbon and water fluxes over a temperate eucalyptus forest and a tropical wet/dry savanna in Australia: measurements and comparison with MODIS remote sensing estimates. *Agric. For. Meteorol.* 129 (3–4), 151–173. <http://dx.doi.org/10.1016/j.agrformet.2004.12.004>.
- Lindauer, M., Schmid, H.P., Grote, R., Mauder, M., Steinbrecher, R., et al., 2014. Net ecosystem exchange over a non-cleared wind-throw-disturbed upland spruce forest—measurements and simulations. *Agric. For. Meteorol.* 197, 219–234. <http://dx.doi.org/10.1016/j.agrformet.2014.07.005>.
- Loubet, B., Laville, P., Lehuger, S., Larmanou, E., Fléchar, C., et al., 2011. Carbon, nitrogen and greenhouse gases budgets over a four years crop rotation in northern France. *Plant Soil* 343 (1–2), 109–137. <http://dx.doi.org/10.1007/s11104-011-0751-9>.
- Lund, M., Falk, J.M., Friberg, T., Mbufong, H.N., Sigsgaard, C., et al., 2012. Trends in CO₂ exchange in a high Arctic tundra heath, 2000–2010. *J. Geophys. Res. Biogeosci.* 117 (2), n/a. <http://dx.doi.org/10.1029/2011JG001901>.
- Ma, S., Baldocchi, D.D., Xu, L., Hehn, T., 2007. Inter-annual variability in carbon dioxide exchange of an oak/grass savanna and open grassland in California. *Agric. For. Meteorol.* 147 (3–4), 157–171. <http://dx.doi.org/10.1016/j.agrformet.2007.07.008>.
- Mao, J., Fu, W., Shi, X., Ricciuto, D.M., Fisher, J.B., et al., 2015. Disentangling climatic and anthropogenic controls on global terrestrial evapotranspiration trends. *Environ. Res. Lett.* 10 (9), 094008. <http://dx.doi.org/10.1088/1748-9326/10/9/094008>.
- Mao, J., Thornton, P.E., Shi, X., Zhao, M., Post, W.M., 2012. Remote sensing evaluation of CLM4 GPP for the period 2000–09. *J. Clim.* 25 (15), 5327–5342. <http://dx.doi.org/10.1175/JCLI-D-11-00401.1>.
- Marañón-Jiménez, S., Castro, J., Kowalski, A.S., Serrano-Ortiz, P., Reverter, B.R., et al., 2011. Post-fire soil respiration in relation to burnt wood management in a Mediterranean mountain ecosystem. *For. Ecol. Manag.* 261 (8), 1436–1447. <http://dx.doi.org/10.1016/j.foreco.2011.01.030>.
- Marchesini, L.B., Papale, D., Reichstein, M., Vuichard, N., Tchekakova, N., et al., 2007. Carbon balance assessment of a natural steppe of southern Siberia by multiple constraint approach. *Biogeosci. Discuss.* 4 (1), 165–208.
- Marcolli, B., Cescatti, A., Montagnani, L., Manca, G., Kerschbaumer, G., et al., 2005. Importance of advection in the atmospheric CO₂ exchanges of an alpine forest. *Agric. For. Meteorol.* 130 (3), 193–206. <http://dx.doi.org/10.1016/j.agrformet.2005.03.006>.
- Matteucci, M., Gruening, C., Godek Ballarin, I., Seufert, G., Cescatti, A., 2015. Components, drivers and temporal dynamics of ecosystem respiration in a Mediterranean pine forest. *Soil Biol. Biochem.* 88, 224–235. <http://dx.doi.org/10.1016/j.soilbio.2015.05.017>.
- Mauder, M., Cuntz, M., Drüe, C., Graf, A., Rebmann, C., et al., 2013. A strategy for quality and uncertainty assessment of long-term eddy-covariance measurements. *Agric. For. Meteorol.* 169, 122–135. <http://dx.doi.org/10.1016/j.agrformet.2012.09.006>.
- McMurtrie, R.E., Norby, R.J., Medlyn, B.E., Dewar, R.C., Pepper, D.A., et al., 2008. Why is plant-growth response to elevated CO₂ optimised when water is limiting, but reduced when nitrogen is limiting? A growth-optimisation hypothesis. *Funct. Plant Biol.* 35 (6), 521. <http://dx.doi.org/10.1071/FP08128>.
- Meir, P., Levy, P., Grace, J., Jarvis, P., 2007. Photosynthetic parameters from two contrasting woody vegetation types in West Africa. *Plant Ecol.* 192 (2), 277–287. <http://dx.doi.org/10.1007/s11258-007-9320-y>.
- Merbold, L., Kutsch, W.L., Corradi, C., Kolle, O., Rebmann, C., et al., 2009. Artificial drainage and associated carbon fluxes (CO₂/CH₄) in a tundra ecosystem. *Glob. Chang. Biol.* 15 (11), 2599–2614. <http://dx.doi.org/10.1111/j.1365-2486.2009.01962.x>.
- Migliavacca, M., Meroni, M., Manca, G., Matteucci, G., Montagnani, L., et al., 2009. Seasonal and interannual patterns of carbon and water fluxes of a poplar plantation under peculiar eco-climatic conditions. *Agric. For. Meteorol.* 149 (9), 1460–1476. <http://dx.doi.org/10.1016/j.agrformet.2009.04.003>.
- Miller, S.D., Goulden, M.L., Menton, M.C., Da Rocha, H.R., De Freitas, H.C., et al., 2004. Biometric and micrometeorological measurements of tropical forest carbon balance. *Ecol. Appl.* 14 (4 suppl.), 114–126. <http://dx.doi.org/10.1890/02-6005>.
- Miralles, D.G., van den Berg, M.J., Gash, J.H., Parinussa, R.M., de Jeu, R.A.M., et al., 2013. El Niño–La Niña cycle and recent trends in continental evaporation. *Nat. Clim. Chang.* 4 (2), 122–126. <http://dx.doi.org/10.1038/nclimate2068>.
- Mkhabela, M.S., Amiro, B.D., Barr, A.G., Black, T.A., Hawthorne, I., et al., 2009. Comparison of carbon dynamics and water use efficiency following fire and harvesting in Canadian boreal forests. *Agric. For. Meteorol.* 149 (5), 783–794. <http://dx.doi.org/10.1016/j.agrformet.2008.10.025>.
- Monteith, J.L., 1972. Solar radiation and productivity in tropical ecosystems. *J. Appl. Ecol.* 9 (3), 747–766.
- Moureaux, C., Debacq, A., Bodson, B., Heinesch, B., Aubinet, M., 2006. Annual net ecosystem carbon exchange by a sugar beet crop. *Agric. For. Meteorol.* 139 (1), 25–39. <http://dx.doi.org/10.1016/j.agrformet.2006.05.009>.
- Mu, Q., Heinsch, F.A., Zhao, M., Running, S.W., 2007. Development of a global evapotranspiration algorithm based on MODIS and global meteorology data. *Remote Sens. Environ.* 111 (3), 519–536. <http://dx.doi.org/10.1016/j.rse.2006.07.007>.
- Mu, Q., Zhao, M., Running, S.W., 2011. Improvements to a MODIS global terrestrial evapotranspiration algorithm. *Remote Sens. Environ.* 115 (8), 1781–1800. <http://dx.doi.org/10.1016/j.rse.2011.02.019>.
- Norby, R.J., Delucia, E.H., Gielen, B., Calfapietra, C., Giardina, C.P., et al., 2005. Forest response to elevated CO₂ is conserved across a broad range of productivity. *Proc. Natl. Acad. Sci. U. S. A.* 102 (50), 18052–18056. <http://dx.doi.org/10.1073/pnas.0509478102>.
- Pavelka, M., Acosta, M., Marek, M.V., Kutsch, W., Janous, D., 2007. Dependence of the Q10 values on the depth of the soil temperature measuring point. *Plant Soil* 292 (1–2), 171–179. <http://dx.doi.org/10.1007/s11104-007-9213-9>.
- Paw U, K.T., 1987. Mathematical analysis of the operative temperature and energy budget. *J. Therm. Biol.* 12 (3), 227–233. [http://dx.doi.org/10.1016/0306-4565\(87\)90009-X](http://dx.doi.org/10.1016/0306-4565(87)90009-X).
- Paw U, K.T., Gao, W., 1988. Applications of solutions to non-linear energy budget equations. *Agric. For. Meteorol.* 43 (2), 121–145. [http://dx.doi.org/10.1016/0168-1923\(88\)90087-1](http://dx.doi.org/10.1016/0168-1923(88)90087-1).
- Peel, M.C., Finlayson, B.L., McMahon, T.A., 2006. Updated world map of the Köppen–Geiger climate classification. *Meteorol. Z.* 15 (3), 259–263. <http://dx.doi.org/10.1127/0941-2948/2006/0130>.
- Piao, S., Sitoh, S., Ciais, P., Friedlingstein, P., Peylin, P., et al., 2013. Evaluation of terrestrial carbon cycle models for their response to climate variability and to CO₂ trends. *Glob. Chang. Biol.* 19 (7), 2117–2132. <http://dx.doi.org/10.1111/gcb.12187>.
- Pilegaard, K., Hummelshøj, P., Jensen, N., Chen, Z., 2001. Two years of continuous CO₂ eddy-flux measurements over a Danish beech forest. *Agric. For. Meteorol.* 107 (1), 29–41. [http://dx.doi.org/10.1016/S0168-1923\(00\)00227-6](http://dx.doi.org/10.1016/S0168-1923(00)00227-6).
- Pirk, N., Mastepanov, M., Parmentier, F.-J.W., Lund, M., Crill, P., et al., 2016. Calculations of automatic chamber flux measurements of methane and carbon dioxide using short time series of concentrations. *Biogeosciences* 13 (4), 903–912. <http://dx.doi.org/10.5194/bg-13-903-2016>.
- Platnick, S., King, M.D., Ackerman, S.A., Menzel, W.P., Baum, B.A., et al., 2003. The MODIS cloud products: algorithms and examples from terra. *IEEE Trans. Geosci. Remote Sens.* 41 (2), 459–473. <http://dx.doi.org/10.1109/TGRS.2002.808301>.
- Plummer, S.E., 2000. Perspectives on combining ecological process models and remotely sensed data. *Ecol. Model.* 129, 169–186. [http://dx.doi.org/10.1016/S0304-3800\(00\)00233-7](http://dx.doi.org/10.1016/S0304-3800(00)00233-7).
- Posse, G., Lewczuk, N., Richter, K., Cristiano, P., 2016. Carbon and water vapor balance in a subtropical pine plantation. *iForest - Biogeosci. For.* 0 (0), e1–e8. <http://dx.doi.org/10.3832/ifor1815-009>.
- Prober, S.M., Thiele, K.R., Rundel, P.W., Yates, C.J., Berry, S.L., et al., 2012. Facilitating adaptation of biodiversity to climate change: a conceptual framework applied to the world's largest Mediterranean-climate woodland. *Clim. Chang.* 110 (1–2), 227–248. <http://dx.doi.org/10.1007/s10584-011-0092-y>.
- Rambal, S., Joffre, R., Ourcival, J.M., Cavender-Bares, J., Rocheteau, A., 2004. The growth respiration component in eddy CO₂ flux from a *Quercus ilex* mediterranean forest. *Glob. Chang. Biol.* 10 (9), 1460–1469. <http://dx.doi.org/10.1111/j.1365-2486.2004.00819.x>.
- Remer, L.A., Kaufman, Y.J., Tanré, D., Mattoo, S., Chu, D.A., et al., 2005. The MODIS aerosol algorithm, products, and validation. *J. Atmos. Sci.* 62 (4), 947–973. <http://dx.doi.org/10.1175/JAS3385.1>.
- Reverter, B.R., Sánchez-Cañete, E.P., Resco, V., Serrano-Ortiz, P., Oyonarte, C., et al., 2010. Analyzing the major drivers of NEE in a Mediterranean alpine shrubland. *Biogeosciences* 7 (9), 2601–2611. <http://dx.doi.org/10.5194/bg-7-2601-2010>.
- Rey, A., Pegoraro, E., Tedeschi, V., De Parri, I., Jarvis, P.G., et al., 2002. Annual variation in soil respiration and its components in a coppice oak forest in Central Italy. *Glob. Chang. Biol.* 8 (9), 851–866. <http://dx.doi.org/10.1046/j.1365-2486.2002.00521.x>.
- Rodell, M., Beaudoin, H.K., L'Ecuyer, T.S., Olson, W.S., Famiglietti, J.S., et al., 2015. The observed state of the water cycle in the early 21st century. *J. Clim.* 28:829–8318. <http://dx.doi.org/10.1175/JCLI-D-14-00555.1>.
- Román, M.O., Schaaf, C.B., Woodcock, C.E., Strahler, A.H., Yang, X., et al., 2009. The MODIS (collection V005) BRDF/albedo product: assessment of spatial representativeness over forested landscapes. *Remote Sens. Environ.* 113 (11), 2476–2498. <http://dx.doi.org/10.1016/j.rse.2009.07.009>.
- Ruehr, N.K., Martin, J.G., Law, B.E., 2012. Effects of water availability on carbon and water exchange in a young ponderosa pine forest: above- and belowground responses. *Agric. For. Meteorol.* 164, 136–148. <http://dx.doi.org/10.1016/j.agrformet.2012.05.015>.
- Running, S.W., Nemani, R.R., Heinsch, F.A., Zhao, M., Reeves, M., et al., 2004. A continuous satellite-derived measure of global terrestrial primary production. *Bioscience* 54 (6), 547. [http://dx.doi.org/10.1641/0006-3568\(2004\)054\[0547:ACSMOG\]2.0.CO;2](http://dx.doi.org/10.1641/0006-3568(2004)054[0547:ACSMOG]2.0.CO;2).
- Ryu, Y., Baldocchi, D.D., Black, T.A., Detto, M., Law, B.E., et al., 2012a. On the temporal upscaling of evapotranspiration from instantaneous remote sensing measurements to 8-day mean daily-sums. *Agric. For. Meteorol.* 152 (1), 212–222. <http://dx.doi.org/10.1016/j.agrformet.2011.09.010>.
- Ryu, Y., Baldocchi, D.D., Kobayashi, H., Van Ingen, C., Li, J., et al., 2011. Integration of MODIS land and atmosphere products with a coupled-process model to estimate gross primary productivity and evapotranspiration from 1 km to global scales. *Glob. Biogeochem. Cycles* 25 (GB4017), 1–24. <http://dx.doi.org/10.1029/2011GB004053>.
- Ryu, Y., Verfaillie, J., Macfarlane, C., Kobayashi, H., Sonntag, O., et al., 2012b. Continuous observation of tree leaf area index at ecosystem scale using upward-pointing digital cameras. *Remote Sens. Environ.* 126, 116–125. <http://dx.doi.org/10.1016/j.rse.2012.08.027>.
- Sabbatini, S., Arriga, N., Bertolini, T., Castaldi, S., Chiti, T., et al., 2016. Greenhouse gas balance of cropland conversion to bioenergy poplar short-rotation coppice. *Biogeosciences* 13 (1), 95–113. <http://dx.doi.org/10.5194/bg-13-95-2016>.
- Sasai, T., Ichii, K., Yamaguchi, Y., Nemani, R., 2005. Simulating terrestrial carbon fluxes using the new biosphere model “biosphere model integrating eco-physiological and mechanistic approaches using satellite data” (BEAMS). *J. Geophys. Res.* 110 (G2), G02014. <http://dx.doi.org/10.1029/2005JG000045>.

- Scanlon, T.M., Albertson, J.D., 2004. Canopy scale measurements of CO₂ and water vapor exchange along a precipitation gradient in southern Africa. *Glob. Chang. Biol.* 10 (3), 329–341.
- Schmid, H.P., Grimmer, C.S.B., Cropley, F., Offerle, B., Su, H.B., 2000. Measurements of CO₂ and energy fluxes over a mixed hardwood forest in the mid-western United States. *Agric. For. Meteorol.* 103 (4), 357–374. [http://dx.doi.org/10.1016/S0168-1923\(00\)00140-4](http://dx.doi.org/10.1016/S0168-1923(00)00140-4).
- Scholes, R.J., Gureja, N., Giannecchini, M., Dovie, D., Wilson, B., et al., 2001. The environment and vegetation of the flux measurement site near Skukuza, Kruger National Park. *Koedoe* 44 (1), 73–83. <http://dx.doi.org/10.4102/koedoe.v44i1.187>.
- Schroder, I., 2014. Arcturus Emerald OzFlux Tower Site. OzFlux: Australian and New Zealand Flux Research and Monitoring (doi:10.2100.100/14249).
- Scott, R.L., 2010. Using watershed water balance to evaluate the accuracy of eddy covariance evaporation measurements for three semiarid ecosystems. *Agric. For. Meteorol.* 150 (2), 219–225. <http://dx.doi.org/10.1016/j.agrformet.2009.11.002>.
- Scott, R., 2016. AmeriFlux US-Wgk Walnut Gulch Kendall Grasslands. AmeriFlux. <http://dx.doi.org/10.17190/AMF/1246112>.
- Seemann, S.W., Li, J., Gumley, L.E., Strabala, K.I., Menzel, W.P., 2003. Operational retrieval of atmospheric temperature, moisture, and ozone from MODIS infrared radiances. In: Menzel, W.P., Zhang, W.-J., Le Marshall, J., Tokuno, M. (Eds.), *Third International Asia-Pacific Environmental Remote Sensing of the Atmosphere, Ocean, Environment, and Space*. International Society for Optics and Photonics, pp. 168–176. <http://dx.doi.org/10.1117/12.466686>.
- Sellers, P.J., Dickinson, R.E., Randall, D.A., Betts, A.K., Hall, F.G., et al., 1997. Modeling the exchanges of energy, water, and carbon between continents and the atmosphere. *Science* 275 (5299), 502–509. <http://dx.doi.org/10.1126/science.275.5299.502>.
- Sellers, P.J., Meeson, B.W., Hall, F.G., Asrar, G., Murphy, R.E., et al., 1995. Remote sensing of the land surface for studies of global change: Models – algorithms – experiments. *Remote Sens. Environ.* 51 (94), 3–26. [http://dx.doi.org/10.1016/0034-4257\(94\)00061-Q](http://dx.doi.org/10.1016/0034-4257(94)00061-Q).
- Senay, G.B., Bohms, S., Singh, R.K., Gowda, P.H., Velpuri, N.M., et al., 2013. Operational evapotranspiration mapping using remote sensing and weather datasets: a new parameterization for the S5EB approach. *J. Am. Water Resour. Assoc.* 49 (3), 577–591. <http://dx.doi.org/10.1111/jawr.12057>.
- Shabanov, N.V., Huang, D., Yang, W., Tan, B., Knyazikhin, Y., et al., 2005. Analysis and optimization of the MODIS leaf area index algorithm retrievals over broadleaf forests. *IEEE Trans. Geosci. Remote Sens.* 43 (8), 1855–1865. <http://dx.doi.org/10.1109/TGRS.2005.852477>.
- Shao, C., Chen, J., Li, L., 2013a. Grazing alters the biophysical regulation of carbon fluxes in a desert steppe. *Environ. Res. Lett.* 8 (2), 025012. <http://dx.doi.org/10.1088/1748-9326/8/2/025012>.
- Shao, P., Zeng, X., Sakaguchi, K., Monson, R.K., Zeng, X., 2013b. Terrestrial carbon cycle: climate relations in eight CMIP5 earth system models. *J. Clim.* 26 (22), 8744–8764. <http://dx.doi.org/10.1175/JCLI-D-12-00831.1>.
- Simard, M., Pinto, N., Fisher, J.B., Baccini, A., 2011. Mapping forest canopy height globally with spaceborne lidar. *J. Geophys. Res. Biogeosci.* 116 (November), 1–12. <http://dx.doi.org/10.1029/2011JG001708>.
- Simioni, G., Gignoux, J., Roux, X.L.E., Benest, D., 2004a. Spatial and temporal variations in leaf area index, specific leaf area and leaf nitrogen of two co-occurring savanna tree species. *Tree Physiol.* 205–216.
- Simioni, G., Le Roux, X., Gignoux, J., Walcroft, A.S., 2004b. Leaf gas exchange characteristics and water- and nitrogen-use efficiencies of dominant grass and tree species in a west African savanna. *Plant Ecol. (Formerly Vegetatio)* 173 (2), 233–246. <http://dx.doi.org/10.1023/B:VEGE.0000029323.74523.80>.
- Sjöström, M., Ardo, J., Eklundh, L., El-Tahir, B.A., El-Khidir, H.A.M., et al., 2008. Evaluation of satellite based indices for primary production estimates in a sparse savanna in the Sudan. *Biogeosci. Discuss.* 5 (4), 2985–3011. <http://dx.doi.org/10.5194/bgd-5-2985-2008>.
- Smith, K.W., Reed, S.C., Cleveland, C.C., Ballantyne, A.P., Anderegg, W.R.L., et al., 2015. Large divergence of satellite and earth system model estimates of global terrestrial CO₂ fertilization. *Nat. Clim. Chang.* <http://dx.doi.org/10.1038/nclimate2879>.
- Song, Y., Ryu, Y., Jeon, S., 2014. Interannual variability of regional evapotranspiration under precipitation extremes: A case study of the Youngsan River basin in Korea. *J. Hydrol.* 519 (PD), 3531–3540. <http://dx.doi.org/10.1016/j.jhydrol.2014.10.048>.
- Spano, D.E.L., Duce, P., Snyder, R.L., Zara, P., Ventura, A., 2005. Assessment of fuel dryness index on Mediterranean vegetation. *Joint Meeting of the 6th Symposium on Fire and Forest Meteorology and 19th Interior West Fire Council Meeting*. American Meteorological Society, Canmore, Canada.
- Still, C.J., 2003. Global distribution of C3 and C4 vegetation: carbon cycle implications. *Glob. Biogeochem. Cycles* 17 (1). <http://dx.doi.org/10.1029/2001GB001807>.
- Sturtevant, C., Ruddell, B.L., Knox, S.H., Verfaillie, J., Matthes, J.H., et al., 2016. Identifying scale-emergent, nonlinear, asynchronous processes of wetland methane exchange. *J. Geophys. Res. Biogeosci.* 121 (1), 188–204. <http://dx.doi.org/10.1002/2015JG003054>.
- Sulman, B.N., Desai, A.R., Cook, B.D., Saliendra, N., Mackay, D.S., 2009. Contrasting carbon dioxide fluxes between a drying shrub wetland in Northern Wisconsin, USA, and nearby forests. *Biogeosciences* 6 (6), 1115–1126. <http://dx.doi.org/10.5194/bg-6-1115-2009>.
- Sundareshwar, P.V., Murtugudde, R., Srinivasan, G., Singh, S., Ramesh, K.J., et al., 2007. Environmental monitoring network for India. *Science* 316 (5822), 204–205.
- Tedeschi, V., Rey, A., Manca, G., Valentini, R., Jarvis, P.J., et al., 2006. Soil respiration in a Mediterranean oak forest at different developmental stages after coppicing. *Glob. Chang. Biol.* 12 (1), 110–121. <http://dx.doi.org/10.1111/j.1365-2486.2005.01081.x>.
- Urbanski, S., Barford, C., Wofsy, S., Kucharik, C., Pyle, E., et al., 2007. Factors controlling CO₂ exchange on timescales from hourly to decadal at Harvard Forest. *J. Geophys. Res.* 112 (G2), G02020. <http://dx.doi.org/10.1029/2006JG000293>.
- van der Molen, M., Gash, J.H., Elbers, J., 2004. Sonic anemometer (co)sine response and flux measurement: II. The effect of introducing an angle of attack dependent calibration. *Agric. For. Meteorol.* 122 (1), 95–109. <http://dx.doi.org/10.1016/j.agrformet.2003.09.003>.
- Verma, S.B., Dobermann, A., Cassman, K.G., Walters, D.T., Knops, J.M., et al., 2005. Annual carbon dioxide exchange in irrigated and rainfed maize-based agroecosystems. *Agric. For. Meteorol.* 131 (1), 77–96. <http://dx.doi.org/10.1016/j.agrformet.2005.05.003>.
- Verma, M., Friedl, M.A., Law, B.E., Bonal, D., Kiely, G., et al., 2015. Improving the performance of remote sensing models for capturing intra- and inter-annual variations in daily GPP: An analysis using global FLUXNET tower data. *Agric. For. Meteorol.* 214–215, 416–429. <http://dx.doi.org/10.1016/j.agrformet.2015.09.005>.
- Verma, M., Friedl, M.A., Richardson, A.D., Kiely, G., Cescatti, A., et al., 2014. Remote sensing of annual terrestrial gross primary productivity from MODIS: An assessment using the FLUXNET La Thuile data set. *Biogeosciences* 11 (8), 2185–2200. <http://dx.doi.org/10.5194/bg-11-2185-2014>.
- Vesala, T., Suni, T., Rannik, Ü., Keronen, P., Markkanen, T., et al., 2005. Effect of thinning on surface fluxes in a boreal forest. *Glob. Biogeochem. Cycles* 19 (2), 1–11. <http://dx.doi.org/10.1029/2004GB002316>.
- Vinukollu, R.K., Meynadier, R., Sheffield, J., Wood, E.F., 2011. Multi-model, multi-sensor estimates of global evapotranspiration: Climatology, uncertainties and trends. *Hydrol. Process.* 25 (26), 3993–4010. <http://dx.doi.org/10.1002/hyp.8393>.
- Wallace, J.M., Hobbs, P.V., 1977. *Atmospheric Science: An Introductory Survey*. Academic Press.
- Wan, Z., 2008. New refinements and validation of the MODIS land-surface temperature/emissivity products. *Remote Sens. Environ.* 112 (1), 59–74. <http://dx.doi.org/10.1016/j.rse.2006.06.026>.
- Wang, K., Dickinson, R.E., Wild, M., Liang, S., 2010. Evidence for decadal variation in global terrestrial evapotranspiration between 1982 and 2002: 1. Model development. *J. Geophys. Res.* 115 (D20), D20112. <http://dx.doi.org/10.1029/2009JD013671>.
- Wang, Y., Law, R.M., Davies, H.L., McGregor, J.L., Abramowitz, G., 2006. The CSIRO Atmosphere Biosphere Land Exchange (CABLE) Model for Use in Climate Models and as an Offline Model.
- Westergaard-Nielsen, A., Lund, M., Hansen, B.U., Tamstorf, M.P., 2013. Camera derived vegetation greenness index as proxy for gross primary production in a low Arctic wetland area. *ISPRS J. Photogramm. Remote Sens.* 86, 89–99. <http://dx.doi.org/10.1016/j.isprsjprs.2013.09.006>.
- Whitley, R., Beringer, J., Hutley, L.B., Abramowitz, G., De Kauwe, M.G., et al., 2016. A model inter-comparison study to examine limiting factors in modelling Australian tropical savannas. *Biogeosciences* 13 (11), 3245–3265. <http://dx.doi.org/10.5194/bg-13-3245-2016>.
- Wohlfahrt, G., Hammerle, A., Haslwanter, A., Bahn, M., Tappeiner, U., et al., 2008. Seasonal and inter-annual variability of the net ecosystem CO₂ exchange of a temperate mountain grassland: Effects of weather and management. *J. Geophys. Res.* 113 (D8), D08110. <http://dx.doi.org/10.1029/2007JD009286>.
- Wolfe, R.E., Roy, D.P., Vermote, E., 1998. MODIS land data storage, gridding, and compositing methodology: Level 2 grid. *IEEE Trans. Geosci. Remote Sens.* 36 (4), 1324–1338. <http://dx.doi.org/10.1109/36.701082>.
- Xu, L., Baldocchi, D.D., 2003. Seasonal trends in photosynthetic parameters and stomatal conductance of blue oak (*Quercus douglasii*) under prolonged summer drought and high temperature. *Tree Physiol.* 23 (13), 865–877. <http://dx.doi.org/10.1093/treephys/23.13.865>.
- Yamazaki, T., Kato, K., Ito, T., Nakai, T., Matsumoto, K., et al., 2013. A common stomatal parameter set used to simulate the energy and water balance over boreal and temperate forests. *Journal of the Meteorological Society of Japan*. Ser. II 91 (3), 273–285. <http://dx.doi.org/10.2151/jmsj.2013-303>.
- Yan, H., Wang, S., Billesbach, D., Oechel, W., Bohrer, G., et al., 2015. Improved global simulations of gross primary product based on a new definition of water stress factor and a separate treatment of C3 and C4 plants. *Ecol. Model.* 297, 42–59. <http://dx.doi.org/10.1016/j.ecolmodel.2014.11.002>.
- Yan, H., Wang, S.Q., Billesbach, D., Oechel, W., Zhang, J.H., et al., 2012. Global estimation of evapotranspiration using a leaf area index-based surface energy and water balance model. *Remote Sens. Environ.* 124, 581–595. <http://dx.doi.org/10.1016/j.rse.2012.06.004>.
- Yan, H., Yu, Q., Zhu, Z.-C., Myneni, R.B., Yan, H.-M., et al., 2013. Diagnostic analysis of inter-annual variation of global land evapotranspiration over 1982–2011: Assessing the impact of ENSO. *Journal of Geophysical Research: Atmospheres* 118 (16), 8969–8983. <http://dx.doi.org/10.1002/jgrd.50693>.
- Yang, Z.L., Niu, G.Y., Mitchell, K.E., Chen, F., Ek, M.B., et al., 2011. The community Noah land surface model with multiparameterization options (Noah-MP): 2. Evaluation over global river basins. *Journal of Geophysical Research: Atmospheres* 116 (12), 1–16. <http://dx.doi.org/10.1029/2010JD015140>.
- Yeber, M., Van Dijk, A.I.J.M., Leuning, R., Guerschman, J.P., 2015. Global vegetation gross primary production estimation using satellite-derived light-use efficiency and canopy conductance. *Remote Sens. Environ.* 163, 206–216. <http://dx.doi.org/10.1016/j.rse.2015.03.016>.
- Yeber, M., Van Dijk, A., Leuning, R., Huete, A., Guerschman, J.P., 2013. Evaluation of optical remote sensing to estimate actual evapotranspiration and canopy conductance. *Remote Sens. Environ.* 129, 250–261. <http://dx.doi.org/10.1016/j.rse.2012.11.004>.
- Yin, X., 2000. A generic equation for nitrogen-limited leaf area index and its application in crop growth models for predicting leaf senescence. *Ann. Bot.* 85 (5), 579–585. <http://dx.doi.org/10.1006/ambo.1999.1104>.
- Yu, G.-R., Wen, X.-F., Sun, X.-M., Tanner, B.D., Lee, X., et al., 2006. Overview of ChinaFLUX and evaluation of its eddy covariance measurement. *Agric. For. Meteorol.* 137 (3–4), 125–137. <http://dx.doi.org/10.1016/j.agrformet.2006.02.011>.
- Yuan, W., Cai, W., Xia, J., Chen, J., Liu, S., et al., 2014. Global comparison of light use efficiency models for simulating terrestrial vegetation gross primary production based

- on the LaThuile database. *Agric. For. Meteorol.* 192–193, 108–120. <http://dx.doi.org/10.1016/j.agrformet.2014.03.007>.
- Yuan, W., Liu, S., Yu, G., Bonnefond, J.-M.M., Chen, J., et al., 2010. Global estimates of evapotranspiration and gross primary production based on MODIS and global meteorology data. *Remote Sens. Environ.* 114 (7), 1416–1431. <http://dx.doi.org/10.1016/j.rse.2010.01.022>.
- Zeng, Z., Piao, S., Lin, X., Yin, G., Peng, S., et al., 2012. Global evapotranspiration over the past three decades: estimation based on the water balance equation combined with empirical models. *Environ. Res. Lett.* 7 (1), 1–8 Retrieved from <http://iopscience.iop.org/1748-9326/7/1/014026/media>.
- Zhang, Y., Guanter, L., Berry, J.A., Joiner, J., van der Tol, C., et al., 2014. Estimation of vegetation photosynthetic capacity from space-based measurements of chlorophyll fluorescence for terrestrial biosphere models. *Glob. Chang. Biol.* 20 (12), 3727–3742. <http://dx.doi.org/10.1111/gcb.12664>.
- Zhang, F., Chen, J.M., Chen, J., Gough, C.M., Martin, T.A., et al., 2012. Evaluating spatial and temporal patterns of MODIS GPP over the conterminous U.S. against flux measurements and a process model. *Remote Sens. Environ.* 124, 717–729. <http://dx.doi.org/10.1016/j.rse.2012.06.023>.
- Zhang, J.-H., Han, S.-J., Yu, G.-R., 2006. Seasonal variation in carbon dioxide exchange over a 200-year-old Chinese broad-leaved Korean pine mixed forest. *Agric. For. Meteorol.* 137 (3), 150–165. <http://dx.doi.org/10.1016/j.agrformet.2006.02.004>.
- Zhang, K., Kimball, J.S., Nemani, R.R., Running, S.W., 2010. A continuous satellite-derived global record of land surface evapotranspiration from 1983 to 2006. *Water Resour. Res.* 46 (May), 1–21. <http://dx.doi.org/10.1029/2009WR008800>.
- Zhang, K., Kimball, J.S., Nemani, R.R., Running, S.W., Hong, Y., et al., 2015. Vegetation greening and climate change promote multidecadal rises of global land evapotranspiration. *Scientific Reports* 5 (October), 15956. <http://dx.doi.org/10.1038/srep15956>.
- Zhao, M., Heinsch, F.A., Nemani, R.R., Running, S.W., 2005. Improvements of the MODIS terrestrial gross and net primary production global data set. *Remote Sens. Environ.* 95, 164–176. <http://dx.doi.org/10.1016/j.rse.2004.12.011>.
- Zimmermann, F., Plessow, K., Queck, R., Bernhofer, C., Matschullat, J., 2006. Atmospheric N- and S-fluxes to a spruce forest—Comparison of inferential modelling and the throughfall method. *Atmos. Environ.* 40 (25), 4782–4796. <http://dx.doi.org/10.1016/j.atmosenv.2006.03.056>.
- Zscheischler, J., Mahecha, M.D., Harmeling, S., Reichstein, M., 2013. Detection and attribution of large spatiotemporal extreme events in Earth observation data. *Ecol. Inf.* 15, 66–73. <http://dx.doi.org/10.1016/j.ecoinf.2013.03.004>.
- Zscheischler, J., Mahecha, M.D., von Buttlar, J., Harmeling, S., Jung, M., et al., 2014. A few extreme events dominate global interannual variability in gross primary production. *Environ. Res. Lett.* 9 (3), 035001. <http://dx.doi.org/10.1088/1748-9326/9/3/035001>.